Mathematical Modeling of the Hot Strip Rolling of Microalloyed Nb, Multiply-Alloyed Cr-Mo, and Plain C-Mn Steels

FULVIO SICILIANO, Jr. and JOHN J. JONAS

Industrial mill logs from seven different hot strip mills (HSMs) were analyzed in order to calculate the mean flow stresses (MFSs) developed in each stand. The schedules were typical of the processing of microalloyed Nb, multiply-alloyed Cr-Mo, and plain C-Mn steels. The calculations, based on the Sims analysis, take into account work roll flattening, redundant strain, and the forward slip ratio. The measured stresses are then compared to the predictions of a model based on an improved Misaka MFS equation, in which solute effects, strain accumulation, and the kinetics of static recrystallization (SRX) and metadynamic recrystallization (MDRX) are fully accounted for. Good agreement between the measured and predicted MFSs is obtained over the whole range of rolling temperatures. The evolution of grain size and the fractional softening are also predicted by the model during all stages of strip rolling. Special attention was paid to the Nb steels, in which the occurrence of Nb(C, N) precipitation strongly influences the rolling behavior, preventing softening between passes. The present study leads to the conclusion that Mn addition retards the strain-induced precipitation of Nb; by contrast, Si addition has an accelerating effect. The critical strain for the onset of dynamic recrystallization (DRX) in Nb steels is derived, and it is shown that the critical strain/peak strain ratio decreases with increasing Nb content; furthermore, Mn and Si have marginal but opposite effects. It is demonstrated that DRX followed by MDRX occurs under most conditions of hot strip rolling; during the initial passes, it is due to high strains, low strain rates, and high temperatures, and, in the final passes, it is a consequence of strain accumulation.

I. INTRODUCTION

THE metallurgical features of plate rolling are now largely understood.[1–10] The long interpass times allow complete static recrystallization (SRX) to take place if the steel is being rolled above the interpass recrystallization stop temperature (T_{nr}), *i.e.*, in the absence of carbonitride precipitation. Plate rolling below T_{nr} leads to austenite pancaking, because strain-induced precipitation prevents any further SRX from occurring. By contrast, during the very short interpass times involved in rod rolling, neither SRX nor precipitation can take place,[11–14] and, in contrast to plate rolling, the strain accumulation that takes place leads to dynamic recrystallization (DRX) followed by metadynamic recrystallization (MDRX). Thus, the metallurgical characteristics of plate rolling, on the one hand, and of rod rolling, on the other hand, are now fairly clear.

From the point of view of interpass time, strip rolling falls between the two processes discussed previously. During the initial passes, when the interpass times are still relatively long, the metallurgical behavior is similar to plate rolling. As the interpass intervals become shorter, the characteristics approach those of rod rolling. Because the classification of strip rolling as being like plate rolling, on the one hand, or like rod rolling, on the other, depends on chemistry and rolling schedule as well as pass number, a relatively simple and generally accepted analysis of this process has not yet been achieved. The goal of the present research was, therefore, to characterize strip rolling in terms of softening mechanism, strain accumulation, grain size, and precipitation. Also, the rolling behavior of microalloyed Nb, plain C-Mn, and some Cr-Mo grades will be considered and compared.

Another important point that arose from this study is that the levels of Mn and Si present in the steel appear to influence the precipitation behavior during strip rolling. The occurrence of precipitation changes the rolling load and must, therefore, be accurately predicted.

Hodgson[15] has carried out an excellent analysis of the different types of mathematical models and has supplied a list of the advantages associated with the application of a particular model to a given practical situation. According to this author, the main advantages are (1) a reduction in the number of mill trials, (2) an evaluation of hardware modifications, (3) the prediction of variables that cannot be measured, (4) an estimation of the effect of interactions, (5) the potential for performance enhancement, and (6) inexpensive research costs.

The applicability of any model must be intensively tested in advance, preferably with industrial data. That is the approach that was employed here. After an improved accuracy in predicting the operational parameters has been demonstrated, the model can then be applied to production.

The analysis of mean flow stress (MFS) behavior as a function of inverse absolute temperature permits identification of the main microstructural changes taking place during rolling. These include SRX, DRX followed by MDRX, strain accumulation, and phase transformation. Figure 1 illustrates these phenomena schematically in the form of an MFS *vs* $1/T$ curve for a hypothetical five-pass schedule. Beginning at the first pass (on the left-hand, or high-temperature side), there is a low-slope region, within which SRX occurs. The

FULVIO SICILIANO, Jr., Research Associate, and JOHN J. JONAS, Professor, are with the Department of Metallurgical Engineering, McGill University, Montreal, PQ, Canada H3A 2B2.

Manuscript submitted March 22, 1999.

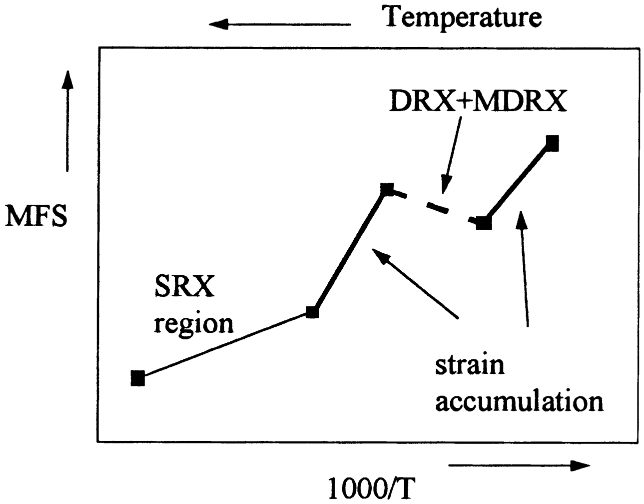

Fig. 1—Schematic representation of the evolution of MFS as a function of the inverse absolute temperature. Each characteristic slope is associated with a distinct metallurgical phenomenon.

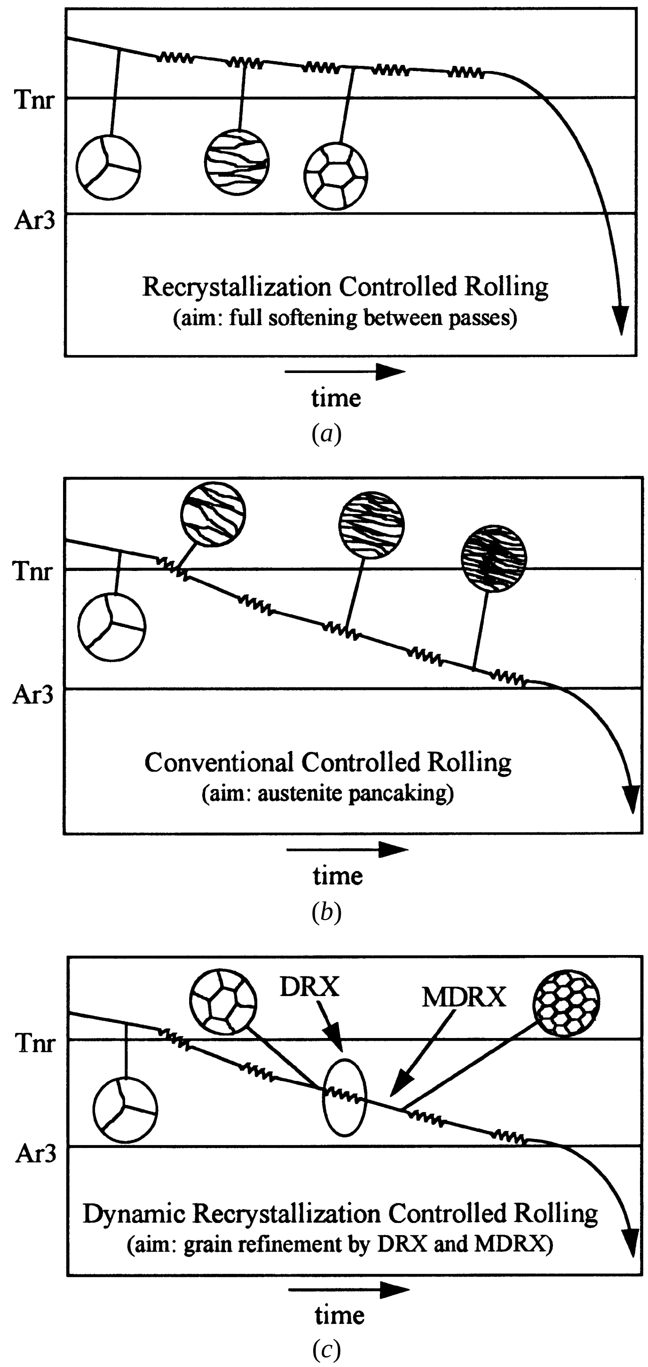

Fig. 2—Temperature-time diagrams comparing three rolling approaches: (*a*) recrystallization controlled rolling, (*b*) conventional controlled rolling, and (*c*) dynamic recrystallization controlled rolling.

high temperature permits full softening to take place during the interpass interval. After pass 2, the lower temperature does not permit full softening, leading to strain accumulation. This accumulation then leads to the onset of DRX (as long as there is no precipitation), which is followed by MDRX between passes 3 and 4.

The analysis of MFS curves as described previously was first proposed by Boratto *et al.*[1] for determination of the three critical temperatures of steel rolling (Ar3, Ar1, and T_{nr}).[2,3,4] This technique has also been used to deduce that DRX occurs in seamless tube rolling[16,17] as well as in hot strip mills (HSMs).[18,19] Sarmento and Evans[19] came to similar conclusions in their analysis of industrial data from two HSMs.

The main types of controlled rolling considered here are listed in the following paragraphs.

Recrystallization-Controlled Rolling. In the schedules considered subsequently, as long as strip rolling is carried out above T_{nr}, SRX is considered to take place. Conversely, below T_{nr}, there is strain accumulation.

Conventional-Controlled Rolling. Here, finishing is employed to flatten or "pancake" the austenite grains at temperatures below T_{nr}. In this case, the particle pinning resulting from the precipitation of Nb(C, N) retards or even prevents the occurrence of recrystallization. In the *absence* of precipitation, as long as rolling is carried out below T_{nr} for *static* recrystallization, the strain accumulation that takes place can trigger DRX followed by MDRX, leading to rapid softening between passes. In terms of mathematical modeling, if there is no precipitation and the accumulated strain exceeds the critical strain, DRX is initiated, often causing full and fast softening. This is usually associated with unpredictable load drops in the final passes.[20]

Dynamic Recrystallization-Controlled Rolling. This type of process consists of inducing DRX in one or more passes during the rolling schedule. This can be done either by applying large single strains to the material or *via* strain accumulation. Both methods allow the total strain to exceed the critical strain for the initiation of DRX. Some of the benefits of this approach involve the intense grain refinement caused by DRX when high strain rates are employed and large strains are applied (this corresponds to single-peak behavior in the stress-strain curve). Circumstantial evidence for the occurrence of DRX in seamless tube rolling[16,17] and HSMs[18,19,21,22] can be found in the literature.

Figure 2 illustrates schematically the three different rolling paradigms described previously for a hypothetical five-pass schedule. The conditions associated with each type of rolling are displayed in Table I. Knowledge of the rolling parameters and process limitations associated with each method makes

Table I. Mechanistic Conditions Pertaining to the Three Controlled Rolling Techniques

Type of Process	T Range with Respect to T_{nr}	Role of Strain-Induced Precipitation	Relation between Precipitation and Recrystallization
RCR	above	absence required	SRX before precipitation
CCR	below	presence required	precipitation before SRX or DRX
DRCR	below	absence required	no SRX; DRX before precipitation

possible the design of rolling schedules to fit the needs and constraints of each case.

II EXPERIMENTAL PROCEDURE

The present work combines the use of models developed from hot torsion test data and from the analysis of industrial mill logs.

A. *Materials*

Various materials were tested and were divided into three groups: microalloyed Nb (group A), multiply alloyed Cr-Mo (group B), and plain C-Mn (group C) steels. Tables II and III list the grades studied here. In group A (Table II), some steels have low Si contents, with the same base composition (*e.g.*, AD5 and AD6 and AD7 and AD8). Other types have different Mn contents, with the same base composition (*e.g.*, AD9 and AD10 and AD2, AD3, and AD4). These grades are used to study the influences of Mn and Si on the precipitation of Nb(C, N) and on the critical strain/peak strain ratio. Table III gives the chemical compositions of some of the multiply alloyed Cr-Mo and plain C-Mn grades studied here. The steels used for the torsion tests are marked with "TT."

B. *Analysis of Mill Log Data*

Logged data were collected from the following five HSMs: Dofasco seven-stand HSM (Hamilton, Canada), Algoma six-stand–2.69-m-wide HSM (Sault Ste. Marie, Canada), Sumitomo seven-stand HSM (Kashima, Japan), Sumitomo seven-stand HSM (Wakayama, Japan), and BHP six-stand HSM (Port Kembla, Australia). Data from two other HSMs were taken from the literature.[19] One is from the Usiminas six-stand HSM in Brazil, and the other is an unidentified seven-stand HSM referred to here as "Davy."

Some 1300 logs were made available for analysis, of which about 300 were examined in detail. The data that were employed consisted of interstand distances, work roll diameters, and pyrometer locations. For each strip, the following data were used: chemical composition, strip width, strip thicknesses before and after all passes (H and h, respectively), work roll rotational speeds, roll forces, and temperatures (mean values) for each pass, according to a model or to entry and exit temperatures.

The previous parameters were then employed to calculate the true strains, strain rates, interpass times, and MFSs, according to the Sims formulation.[4,23] The corrections for roll flattening,[24,25] redundant strain, and forward slip between roll and strip[25] were taken into account in these

Table II. Chemical Compositions of the Niobium Steels Investigated (Group A)

Steel	Plant	C	Mn	Si	Nb	Ti	N*	Al	P	S
AA1^{TT}	Algoma	0.05	0.35	0.010	0.035	—	0.004	0.043	0.008	0.006
AA2	Algoma	0.05	0.70	0.100	0.053	—	0.005	0.045	0.007	0.004
AA3	Algoma	0.06	0.70	0.110	0.058	—	0.005	0.045	0.008	0.004
AS1^{TT}	Sumitomo	0.07	1.12	0.050	0.023	0.016	0.000	0.029	0.019	0.002
AS2^{TT}	Sumitomo	0.09	1.33	0.060	0.036	0.016	0.003	0.019	0.017	0.020
AB	BHP	0.11	1.05	0.010	0.031	—	0.003	0.040	0.012	0.012
AD1	Dofasco	0.06	0.65	0.225	0.020	—	0.004	0.035	0.008	0.005
AD2	Dofasco	0.14	0.65	0.225	0.020	—	0.004	0.035	0.008	0.005
AD3	Dofasco	0.12	0.85	0.225	0.020	—	0.004	0.035	0.008	0.005
AD4	Dofasco	0.12	1.00	0.225	0.020	—	0.004	0.035	0.008	0.005
AD5	Dofasco	0.06	0.65	0.115	0.030	—	0.004	0.035	0.008	0.005
AD6	Dofasco	0.06	0.65	0.010	0.030	—	0.004	0.035	0.008	0.005
AD7	Dofasco	0.06	0.65	0.115	0.045	—	0.004	0.035	0.008	0.005
AD8	Dofasco	0.06	0.65	0.010	0.045	—	0.004	0.035	0.008	0.005
AD9	Dofasco	0.06	0.45	0.010	0.008	—	0.004	0.035	0.008	0.005
AD10	Dofasco	0.06	0.65	0.010	0.008	—	0.004	0.035	0.008	0.005
AD11	Dofasco	0.06	1.25	0.325	0.075	0.024	0.004	0.035	0.008	0.005
AD12	Dofasco	0.06	1.25	0.325	0.080	—	0.004	0.035	0.008	0.005
AM1	"Davy"	0.06	0.70	0.070	0.050	—	0.004	0.051	0.018	0.013
AM2	"Davy"	0.05	0.45	0.020	0.020	—	0.005	0.047	0.014	0.008
AU	Usiminas	0.11	0.54	0.002	0.018	—	0.004	0.057	0.014	0.008

*For the Dofasco grades, a mean value of 40 ppm N is listed here. The actual values are taken into account in the spreadsheets.

Table III. Chemical Compositions of the Multiply-Alloyed and Plain C-Mn Steels

Group	Steel	Plant	C	Mn	Si	Nb	Ti	Cr	Mo	V	Ni	N	Al	P	S
B	BCM	Sumitomo	0.28	0.52	0.220	—	—	0.83	0.15	—	—	0.005	0.026	0.016	0.004
	BCMV	Sumitomo	0.41	0.63	0.280	—	0.015	1.38	0.60	0.27	0.02	0.006	0.046	0.013	0.001
	BCMVN	Sumitomo	0.47	0.66	0.170	0.016	0.016	0.98	0.97	0.12	0.46	0.004	0.042	0.016	0.004
C	CA^{TT}	Algoma	0.03	0.27	0.010	—	—	—	—	—	—	0.004	0.042	0.008	0.010
	CS1^{TT}	Sumitomo	0.10	1.08	0.060	—	—	—	—	—	—	0.003	0.020	0.017	0.003
	CS2	Sumitomo	0.45	0.76	0.210	—	—	—	—	—	—	0.005	0.004	0.017	0.004
	CD	Dofasco	0.06	0.27	0.000	—	—	—	—	—	—	0.004	0.035	0.007	0.005
	CM	"Davy"	0.03	0.24	0.020	—	—	—	—	—	—	0.004	0.042	0.009	0.006
	CU	Usiminas	0.05	0.24	0.002	—	—	—	—	—	—	0.004	0.030	0.016	0.010

calculations and were organized using MICROSOFT EXCEL* spreadsheet software. Some typical spreadsheet inputs and outputs are shown in Table IV. The same spreadsheet was used for the microalloyed Nb, multiply alloyed Cr-Mo, and plain C-Mn grades; this is because it does not consider microstructure but only mechanical parameters.

* MICROSOFT and EXCEL are trademarks of the Microsoft Corporation, Redmond, WA.

III. THE SUBMODELS APPLIED TO HOT STRIP ROLLING

A. *The MFS Model*

Improvement of the Misaka equation

Misaka's equation[26] has often been employed to specify the MFS for C-Mn steels during hot strip rolling. It will be used here as the basis for a modified equation that takes into account the effects of different alloying elements, such as Mn, Nb, and Ti. The Misaka equation is displayed in Eq. [1]; here, the MFS (σ_M) is a function of the strain, strain rate, temperature, and carbon content in weight percent.

$$\sigma_M = \exp\left(0.126 - 1.75\text{C} + 0.594\text{C}^2 + \frac{2851 + 2968\text{C} - 1120\text{C}^2}{T}\right)\varepsilon^{0.21}\dot{\varepsilon}^{0.13} \quad [1]$$

According to the present method, the Sims formulation is employed to calculate and plot the MFS *vs* 1000/*T* for several bars. Because strip rolling reductions are applied at various strains and strain rates, all the derived MFSs are "normalized" to $\varepsilon = 0.4$ and $\dot{\varepsilon} = 5\ \text{s}^{-1}$.[27,28]

An example of this approach for grade D5 is illustrated in Figure 3. It can be seen that Misaka's equation overpredicts the MFSs obtained from the mill logs for this 0.03 pct Nb steel. On the other hand, it underpredicts the MFSs for some higher Nb grades.[28] The trend of the Misaka equation fits the mill log values reasonably well in the region where the slope is quite shallow (*i.e.*, at low 1/*T* or high *T* values). This indicates that full SRX is occurring between the passes

Table IV. Example of the Spreadsheet Calculations Carried Out Using the Mill Data

Inputs: Data from mill logs

Pass	Roll Radius (mm)	Roll Speed (rpm)	Width (mm)	Gage (mm)	Temperature (°C)	Roll Force (Tonne)
—	—	—	—	30.60	—	—
F1	394	33.9	1264	17.33	987	2157
F2	391	54.5	1264	10.79	951	2223
F3	381	79.2	1264	7.42	915	2116
F4	365	119.0	1264	5.10	907	1691
F5	363	147.1	1264	3.90	896	1357
F6	376	167.2	1264	3.14	884	1264
F7	378	172.0	1264	2.61	872	1627

Outputs

Pass	Hitchcock R' (mm)	Forward Slip Factor	Nominal Strain	Total Strain*	Strain Rate (s^{-1})	Interpass Time (s)	1000/*T* (K^{-1})	Sims MFS (MPa)
F1	403	1.10	0.66	0.75	12.9	3.48	0.79	116
F2	412	1.09	0.55	0.61	25.2	2.14	0.82	151
F3	416	1.08	0.43	0.48	41.3	1.48	0.84	179
F4	402	1.08	0.43	0.47	72.7	1.01	0.85	151
F5	428	1.06	0.31	0.34	94.2	0.79	0.86	178
F6	472	1.05	0.25	0.27	115	0.63	0.86	185
F7	561	1.04	0.21	0.23	131	—	0.87	250

*Includes the redundant strain.

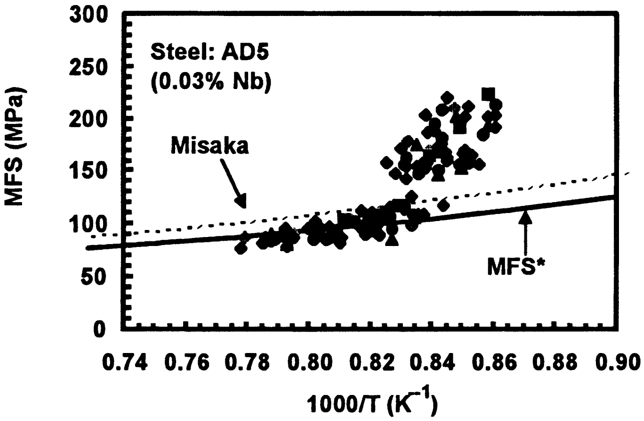

Fig. 3—Comparison of Misaka's equation and the present equation (MFS*) based on chemical composition and fitted to the mill (Sims) data in the SRX region. Here, the mill data for grade AD5 (0.03 pct Nb) are corrected to a constant strain of 0.4 and a constant strain rate of 5 s^{-1}.

in this region. A solution-strengthening factor can, therefore, be added that allows Misaka's equation to fit all grades. For compositions AS1, AS2, and AB, for example, a correction for solute strengthening due to the high Mn content (1.12, 1.33, and 1.08, respectively), allows Misaka's equation to fit the mill values.[28] Another correction is still required for the occurrence of strain accumulation and DRX, which leads to departures from Misaka-type behavior at high values of $1/T$ (*i.e.*, low T). For this purpose, the model by Yada and Senuma[29,30,31] was adapted and tested.[25,27,29] This produced the following final MFS equation:

$$\begin{aligned} \text{MFS}^{+}_{\text{Nb}} = (&\text{MFS}_{\text{Misaka}} (0.768 + 0.51\text{Nb} + 0.137\text{Mn} \\ &+ 4.217\text{Ti})) \times (1 - X_{\text{dyn}}) + K\sigma_{ss}X_{\text{dyn}} \end{aligned} \quad [2]$$

Here, X_{dyn} is the softening attributable to DRX, σ_{ss} is the steady-state stress, and $K = 1.14$ is a parameter that converts flow stress to MFS.

Equation [2] is valid over the following concentration ranges: 0.020 to 0.080 pct Nb, 0.35 to 1.33 pct Mn, and 0 to 0.024 pct Ti. This approach has been used successfully to calculate the MFSs in plain C-Mn[25,27] as well as in Cr-Mo steels,[27,32] and the respective equations are displayed in Eqs. [3] and [4], respectively

$$\begin{aligned} \text{MFS}^{+}_{\text{C-Mn}} = (&\text{MFS}_{\text{Misaka}} (0.768 + 0.137\text{Mn})) \\ &\times (1 - X_{\text{dyn}}) + K\sigma_{ss}X_{\text{dyn}} \end{aligned} \quad [3]$$

The Mn concentrations studied ranged from 0.27 to 1.08 pct. For the multiply alloyed steels, the following relation is applicable:[27,32]

$$\begin{aligned} \text{MFS}^{+}_{\text{Cr-Mo}} = (&\text{MFS}_{\text{Misaka}} (0.835 + 0.51\text{Nb} + 0.098\text{Mn} \\ &+ 0.128\text{Cr}^{0.8} + 0.144\text{Mo}^{0.3} + 0.175\text{V} \\ &+ 0.01\text{Ni})) \times (1 - X_{\text{dyn}}) + K\sigma_{ss}X_{\text{dyn}} \end{aligned} \quad [4]$$

Equation [4] is considered to apply to the following composition ranges: 0.52 to 0.66 pct Mn, 0 to 0.08 pct Nb, 0.83 to 1.38 pct Cr, 0 to 0.46 pct Ni, 0.15 to 0.97 pct Mo, and 0 to 0.27 pct V. Due to the high maximum concentrations of Cr and Mo, the solution effects approached "saturation;" this is why exponents are employed in this expression. The effects of the other elements are considered to be linear over their concentration intervals.*

* Comparison of Tables II and III indicates that the Eq. [2] (group A) steels (Table II) have only *half* the average Si levels (about 0.11) compared to the Eq. [4] (group B) steels of Table III (about 0.22 pct Si). At the time this analysis was carried out, no account was taken of the Si levels on the MFS and, therefore, on the rolling load. In retrospect, however, this would have been desirable, as it appears from a study of the previous relations that the introduction of such a term may have permitted the use of a *single* set of coefficients.

B. *Modeling of Grain Size and Fractional Softening*

During a particular pass of a rolling schedule, the sum of the retained and applied strains will determine which softening mechanism (SRX or DRX + MDRX) will operate. Depending on the type of softening, different equations are then employed to specify the grain size and fractional softening. In this section, a method is described that can be used to follow the microstructural evolution during multipass rolling. For now, no attention is paid to the exact onset of DRX, and the critical strain is simply taken as a fixed fraction of the peak strain. The example given subsequently involves modeling microstructural evolution in a plain C-Mn grade, and the critical strain is considered to be 0.8 ε_p. The onset of DRX in Nb steels is discussed in the next section, IIIC.

During rolling, the temperature decreases continuously. Thus, the temperature adopted for each interpass interval is taken as the average of the prior and subsequent pass temperatures. This assumption is employed because the present equations were derived for isothermal conditions and the interpass times are short enough to allow the use of a single temperature value.

In the present work, the recrystallization and grain-size relations described subsequently were incorporated into the MICROSOFT EXCEL spreadsheet software, as shown in more detail in Section IV. The submodels involved here were assembled by following a method developed for rod rolling.[11] The recrystallization kinetics equations used here are adaptations of the Avrami–Johnson–Mehl–Kolmogorov equation, with parameters that were selected to fit the mill data.

1. *Softening between passes*

A softening model uses parameters such as strain, strain rate, initial grain size, and temperature to decide upon the mechanism and calculate the extent of softening. In an HSM, the softening between passes can be calculated with the aid of an MFS equation and temperature corrections. In the present work, the microstructural evolution equations were tested directly using the spreadsheet for the three groups of steels. The $t_{0.5}$ equation selected for each group is shown in Table V.

Note that Eq. [6] is the only one available for the DRX kinetics of Nb steels. A similar expression is employed for the multiply alloyed grades, as derived in a recent study.[32] For the C-Mn steels, several equations are available; however, the one developed by Hodgson *et al.*[33,36] provided the best fit to the mill logs.

2. *Strain accumulation between passes*

Partial recrystallization between passes results in retained strain, which must be added to the strain applied in the

Table V. Equations Describing the Softening Kinetics

Group	Type	Equation		Reference
A	SRX	$t_{0.5}^{SRX} = (-5.24 + 550\,[Nb]) \times 10^{-18} \varepsilon^{(-4.0+77[Nb])}\, d_0^2 \exp(330{,}000/RT)$	[5]	33
	DRX	$t_{0.5}^{MDRX} = 4.42 \times 10^{-7} \dot{\varepsilon}^{(-0.59)} \exp(153{,}000/RT)$	[6]	34,35
B	SRX	$t_{0.5} = 1.57 \times 10^{-14} \cdot d_0^2 \cdot \varepsilon^{-2.9} \exp\left(\frac{271{,}000}{RT}\right)$	[7]	32
	DRX	$t_{0.5} = 1.84 \times \left[\dot{\varepsilon} \cdot \exp\left(\frac{330{,}000}{RT}\right)\right]^{-0.86} \exp\left(\frac{271{,}000}{RT}\right)$	[8]	32
C	SRX	$t_{0.5}^{SRX} = 2.3 \times 10^{-15} \varepsilon^{-2.5}\, d_0^2 \exp\left(\frac{230{,}000}{RT}\right)$	[9]	32,36
	DRX	$t_{0.5}^{MDRX} = 0.4\left(\dot{\varepsilon} \cdot \exp\left(\frac{300{,}000}{RT}\right)\right)^{-0.8} \exp\left(\frac{240{,}000}{RT}\right)$	[10]	14

subsequent stand. The accumulated strain in pass i ($i > 1$) then becomes[37]

$$\varepsilon_i^a = \varepsilon_i + K_{acc}(1 - X_{i-1})\varepsilon_{i-1} \qquad [11]$$

where X is the fractional softening and K_{acc} is a constant. The value of K_{acc} was reported in the literature as falling between 0.5 and 1.[11,37] The parameter K_{acc} can be related to the rate of recovery. High rates of recovery result in less accumulated strain. This is clear from the work of Gibbs *et al.*,[37] where longer interpass times led to $K_{acc} = 0.5$ and shorter interpass times (less recovery) to $K_{acc} = 1$. In the present hot strip model, the K_{acc} constant is assumed to be 1 and the accumulated strain is used in all the calculations. The latter is considered to represent the average strain present within the material.

3. *Grain-size evolution*

a. *Recrystallized grain size*

This calculation simply takes into account the initial grain size, strain, and/or strain rate. The grain size after SRX is well known to be strongly dependent on the prior strain and only depends on the strain rate to a minor extent. On the other hand, the grain sizes after MDRX are strongly dependent on the strain rate.[14,15,34–36,38–41] The equations used here are listed in Table VI.

The grain size pertaining to the entrance of a given pass is considered to be the "initial" grain size (d_0). Note that the equations used to model the recrystallized grain sizes for the steels pertaining to groups A and B are the same; this is due to the lack of appropriate equations for the multiply alloyed steels.

In the case of incomplete recrystallization, the initial grain size for the following pass (d_{0i+1}) can be calculated using the following relation,[11,33,43] which specifies a kind of "average" derived from the freshly formed and original grain sizes:

$$d_{0_{i+1}} = d_{rex_i} \times X_i^{4/3} + d_{0_i}(1 - X_i)^2 \qquad [18]$$

With this formulation, when X_i is close to 1, the initial grain size for the following pass is d_{rexi}. On the other hand, if X_i is small, d_{0i+1} will be close to the original grain size, d_{0i}; in the latter case, the grains only change their shapes because of the applied strain.[11]

b. *Grain growth after recrystallization*

After complete recrystallization, the microstructure is subjected to grain growth; this is driven by the decrease in free energy associated with the grain boundaries. For the group A and B steels, one single equation (Eq. [19]) was employed to describe grain growth:

$$d^{4.5} = d_0^{4.5} + 4.1 \times 10^{23} \times t_{ip} \times \exp(-435{,}000/RT) \qquad [19]$$

Although the previous equation was derived for Nb steels, it is used here to describe grain growth in the multiply alloyed steels as well. This is due to the lack of an equation for the multiply alloyed grades, and because the alloying elements present in the group B grades make it more reasonable to adopt an equation derived for Nb steels than one derived for C-Mn grades. The grain-growth kinetics in Nb and multiply alloyed steels are, of course, expected to be slower than in plain C-Mn compositions due to solute drag. For the group C (C-Mn) steels, however, a group of equations is available to describe grain growth. The method used here was proposed by Hodgson *et al.*[11,36,44] and is a "pragmatic" one, based on both laboratory[44] and industrial[11] observations.

It should be noted that there is a large difference between the rate of growth during the first second of the interpass interval and the remaining time. This difference may arise because of the large driving force for grain growth present in the initially fine-grained structure. Another possible effect concerns the presence of "deformation" vacancies immediately after rolling, which could accelerate growth.[45] This transition was handled by adopting different grain-growth exponents for each stage[11] and by using the following equations.

Table VI. Equations Describing the Recrystallized Grain Size

Group	Type	Equation		Ref.
A	SRX	$d_{SRX} = 1.1 \cdot d_0^{0.67} \cdot \varepsilon^{-0.67}$	[12]	42
	DRX	$d_{MDRX} = 1370 \times \varepsilon^{-0.13} \exp\left(\frac{-45{,}000}{RT}\right)$	[13]	34
B	SRX	$d_{SRX} = 1.1 \cdot d_0^{0.67} \cdot \varepsilon^{-0.67}$	[14]	41
	DRX	$d_{MDRX} = 1370 \times \varepsilon^{-0.13} \exp\left(\frac{-45{,}000}{RT}\right)$	[15]	35
C	SRX	$d_{SRX} = 343 \cdot d_0^{0.4} \cdot \varepsilon^{-0.5} \exp\left(\frac{-45{,}000}{RT}\right)$	[16]	33,36
	DRX	$d_{MDRX} = 2.6 \times 10^4 \cdot \left(\dot{\varepsilon} \cdot \exp\left(\frac{300{,}000}{RT}\right)\right)^{-0.23}$	[17]	33,36

SRX, $t_{ip} < 1$ s [20]

$$d^2 = d_{SRX}^2 + 4.0 \times 10^7 \,(t_{ip} - 4.32\, t_{0.5}) \exp\left(\frac{-113{,}000}{RT}\right)$$

MDRX, $t_{ip} < 1$ s [21]

$$d^2 = d_{MDRX}^2 + 1.2 \times 10^7 \,(t_{ip} - 2.65\, t_{0.5}) \exp\left(\frac{-113{,}000}{RT}\right)$$

SRX, $t_{ip} > 1$ s [22]

$$d^7 = d_{SRX}^7 + 1.5 \times 10^{27} \,(t_{ip} - 4.32\, t_{0.5}) \exp\left(\frac{-400{,}000}{RT}\right)$$

MDRX, $t_{ip} > 1$ s [23]

$$d^7 = d_{MDRX}^7 + 8.2 \times 10^{25} \,(t_{ip} - 2.65\, t_{0.5}) \exp\left(\frac{-400{,}000}{RT}\right)$$

4. *Design of the microstructural-prediction spreadsheet*

The previous equations describing the microstructural events can now be organized into a spreadsheet. Basically, the spreadsheet parameters displayed in Table VII are used as input data to simulate the microstructural changes taking place during hot rolling, in a pass-by-pass analysis. The starting grain size (after roughing and before strip rolling) is adopted as 100 μm for the C-Mn grades and as 80 μm for the others. The subsequent grain sizes are calculated after recrystallization and grain growth, and the results constitute the input data for the next pass. Both the accumulated strain as well as the redundant strain are employed throughout the calculations. Some typical inputs and outputs of the microstructural-evolution spreadsheet are given in Table VII. The following example uses data from the Dofasco HSM, grade CD.

In C-Mn steels, mechanisms such as carbonitride precipitation followed by strain accumulation do not take place, so only SRX as well as DRX + MDRX effects are considered here. The observed MFS is calculated using the Sims formulation (from the mill data). Then, predictions are made using Eq. [3], based on the Misaka equation. The observed and predicted MFSs are compared in Table VIII, where the differences between the three sets of MFSs are also shown (in percentage).

The "basic" version of the prediction spreadsheet described previously, allowing for strain accumulation and DRX + MDRX, is considered to be fully applicable to the group C (C-Mn) grades. However, for Nb steels, the critical strain for the initiation of DRX must be accurately known, and agreement regarding this quantity is lacking in the literature. The actual precipitation start time during hot strip rolling is also an unknown quantity. In the next two sections (C and D), some improved methods for the estimation of these two parameters will, therefore, be proposed and described for the Nb grades.

C. *Critical Strain for the Initiation of DRX*

The critical strain for the onset of DRX is an important parameter employed in the mathematical modeling of microstructural evolution and of rolling load. Knowledge of the critical strain for the initiation of DRX is a requirement for prediction of the operating softening mechanisms in hot working processes.

For the present purpose, it is useful to express the critical strain for the initiation of DRX (ε_c) as a function of the peak strain (ε_p), as determined from a stress-strain curve. This is because several equations are available to specify the peak strain as a function of initial grain size, temperature, and strain rate for Nb steels. The $\varepsilon_c/\varepsilon_p$ ratio often lies between 0.67 and 0.86[46] and is generally considered to be 0.8 for plain C-Mn steels. Previous workers have reported values for Nb steels as low as 0.65.[34] The effects of Nb, Mn, and Si were taken into account in a recent investigation,[47] and a fit was found for the $\varepsilon_c/\varepsilon_p$ ratio. The method used was to test several possible values of $\varepsilon_c/\varepsilon_p$ and then to select the ratio that provides the best fit to the Sims MFS curve. This procedure, thus, specifies the conditions under which DRX will occur. Over 100 mill logs were tested in this way using the grades listed in Table I. The resulting

Table VII. Spreadsheet Calculation of Grain Size and Fractional Softening in Steel CD, Containing 0.06 Pct C, 0.27 Pct Mn, 0.007 Pct P, and 0.035 Pct Al

Inputs		Steel:CD			
Pass	d_0* (μm)	T (°C)	$\dot{\varepsilon}$ (s^{-1})	t_{ip} (s)	ε**
F 1	100	1003	11.8	3.27	0.60
F 2	—	975	19.0	2.25	0.47
F 3	—	959	30.0	1.62	0.43
F 4	—	941	41.3	1.24	0.34
F 5	—	926	61.1	0.93	0.33
F 6	—	909	82.4	0.73	0.28
F 7	—	895	88.7	—	0.19

Outputs	Steel: CD										
Pass	d_0 (μm)	ε_a	ε_c	$\varepsilon_a > \varepsilon_c$?	$\varepsilon_{0.5}$	X_{dyn}	$t_{0.5}$ (s)	X	d if $X > 0.95$ (μm)	d after t_{ip} (μm)	1000/T (K^{-1})
F 1	100.0	0.60	0.44	Y	0.61	0.17	0.06	1.00	20.5	26.2	0.78
F 2	26.2	0.47	0.35	Y	0.50	0.16	0.04	1.00	16.3	22.3	0.80
F 3	22.3	0.43	0.38	Y	0.53	0.06	0.03	1.00	13.4	19.6	0.81
F 4	19.6	0.34	0.42	—	—	—	0.12	1.00	21.8	29.0	0.82
F 5	29.0	0.33	0.54	—	—	—	0.39	0.81	24.4	19.4	0.83
F 6	19.4	0.34	0.54	—	—	—	0.22	0.9	19.2	16.9	0.85
F 7	16.9	0.22	0.54	—	—	—	0.54	—	21.8	—	0.86

*estimated
**Includes the redundant strain.

Table VIII. Comparison between the Mill (Sims) MFS and the MFS Values Predicted According to the Present Modified Misaka Equation (MFS+) and the Original Equation (Steel: CD)

Pass	Temperature (°C)	1000/T (K^{-1})	Sims MFS (MPa)	MFS+ (MPa)	Difference (Pct)	Misaka MFS (MPa)	Difference (Pct)
F1	1003	0.78	113	118	4.8	134	18.6
F2	975	0.80	128	126	−1.1	143	11.5
F3	959	0.81	134	133	−0.3	154	14.8
F4	941	0.82	133	136	2.5	158	19.2
F5	928	0.83	143	147	2.3	171	19.4
F6	909	0.85	148	159	7.3	178	20.1
F7	895	0.86	165	152	−7.8	171	4.1

relation relies on the peak strain equation derived by Roucoules *et al.*[34] and improved by Minami *et al.*[28]

$$\varepsilon_p = ((1 + 20\text{Nb})/1.78) \times 2.8 \times 10^{-4} \times d_0^{0.5}\left(\dot{\varepsilon} \times \exp\left(\frac{375{,}000}{RT}\right)\right)^{0.17} \quad [24]$$

Here, d_0 is the initial grain size. The $\varepsilon_c/\varepsilon_p$ ratio is then given by

$$\varepsilon_c/\varepsilon_p = 0.8 - 13\text{Nb}_{\text{eff}} + 112\text{Nb}_{\text{eff}}^2 \quad [25]$$

where Nb_{eff} is specified by

$$\text{Nb}_{\text{eff}} = \text{Nb} - \frac{\text{Mn}}{120} + \frac{\text{Si}}{94} \quad [26]$$

Plotting the $\varepsilon_c/\varepsilon_p$ ratio against the *effective* Nb concentration (Eq. [26]) results in a clear relationship. Equations [25] and [26] are considered to apply over the following composition ranges: 0.010 to 0.058 pct Nb, 0.35 to 1.33 pct Mn, and 0.01 to 0.23 pct Si. They describe the progressive decrease in $\varepsilon_c/\varepsilon_p$ ratio represented by the line in Figure 4.

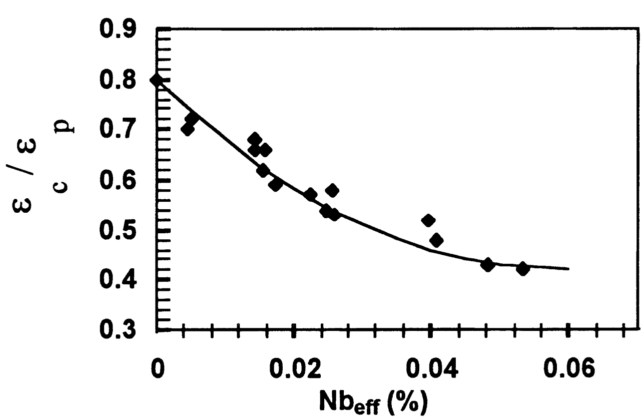

Fig. 4—Dependence of $\varepsilon_c/\varepsilon_p$ ratio on effective Nb concentration as calculated from Eqs. [25] and [26].

The opposite effects of Mn and Si in this equation reflect their opposite effects on Nb diffusivity in austenite[48] and, therefore, on Nb solute drag at grain boundaries.[47] The previous relation is used to predict the occurrence of DRX in the spreadsheet analysis.

D. *Precipitation Model for the Hot Strip Rolling of Nb Steels*

The Dutta and Sellars (DS) model[49] describes the isothermal strain-induced precipitation of Nb(C, N) from supersaturated austenite. The time for 5 pct precipitation is obtained from the relation shown subsequently, which specifies the dependence of the precipitation start time (t_{ps}) in Nb steels on process variables such as the strain, strain rate, and temperature. It also includes the Nb concentration as well as the supersaturation ratio (K_s). The latter, which determines the "driving force" for precipitation, is expressed as

$$K_s = \frac{10^{-6770/T_{RH}+2.26}}{10^{-6770/T_{pass}+2.26}} \qquad [27]$$

where the parameters T_{RH} and T_{pass} are the absolute reheat and pass temperatures. The solubility products that apply to the reheat and pass temperatures are taken from the relation derived by Irvine *et al.*[50] The K_s term expresses the ratio of the amounts of Nb and C in solution at the reheat and pass temperatures, under equilibrium conditions. The final equation is

$$t_{ps} = A\,\mathrm{Nb}^{-1}\varepsilon^{-1}Z^{-0.5}\exp\frac{270{,}000}{RT}\exp\frac{B}{T^3\ln K_s^2} \qquad [28]$$

The values of the constants $A = 3 \times 10^{-6}$ and $B = 2.5 \times 10^{10}$ (K^3) were established by Dutta and Sellars by fitting to published data. The constant B is basically a product of constants and its value is not critical. However, the constant A represents the number of precipitate nuclei per unit volume, which is greatly affected by the strain and temperature. The effect of Mn addition in retarding precipitation[51] was not accounted for in this model and it, therefore, usually needs some fine tuning in order to predict with accuracy the precipitation start times during hot rolling.

In a recent analysis,[52] the DS model was applied to the hot strip rolling or Nb grades. After modification, the model fitted mill data reasonably well. In this case, the DS model was "tuned" by the addition of correction factors that allow for the effects of Si and Mn levels on the precipitation kinetics. The correction factor is the denominator in Eq. [29].

$$t_{ps} = \frac{t_{ps}^{DS}}{10^{(-0.26-0.90\mathrm{Mn}+2.85\mathrm{Si})}} \qquad [29]$$

Two further points are included in the present treatment: (1) the effects of Si and Mn additions on the solubility of Nb carbonitride, and (2) the correction term added to the DS equation to take these effects into account. These modifications will now be described.

1. *Nb carbonitride solubility product*

The solubility equation derived by Irvine *et al.*,[50] which has been used in numerous applications, is shown subsequently. Note that the equation is written for the "equivalent carbon content" = C + 12/14 N.

Table IX. **Published Data for the Solution Temperature of Nb Carbonitride**

Author	C	Mn	Nb	Si	T_{sol} (°C)
Irvine *et al.*[50]	0.10	0.60	0.03	0.30	1098
Meyer[53]	0.06	1.20	0.035	0.07	926
Akben *et al.*[51]	0.05	0.42	0.035	0.25	1026
	0.05	1.25	0.035	0.27	996
	0.06	1.90	0.035	0.26	990
Johansen *et al.*[54]	0.06	0.01	0.035	0.01	1045
Kazinsky *et al.*[55]	0.06	1.00	0.035	0.35	1072

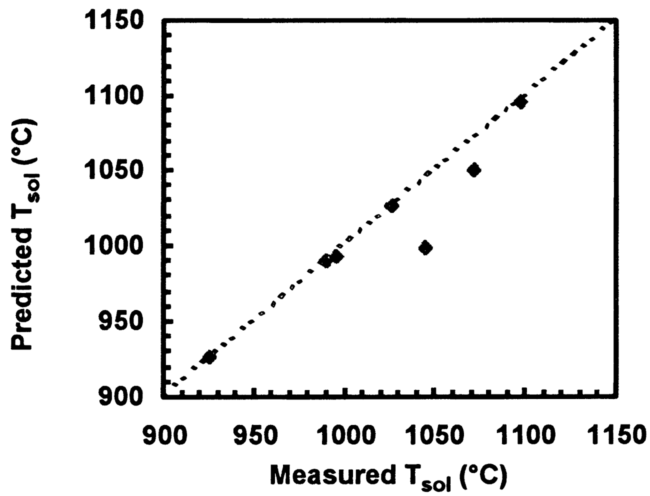

Fig. 5—Comparison of predicted (Eq. [31]) and published solution temperatures for the steels listed in Table VI.

$$\log \mathrm{Nb} \times (\mathrm{C} + 12/14\ \mathrm{N}) = 2.26 - \frac{6770}{T} \qquad [30]$$

This equation was derived for a steel containing 0.6 pct Mn and 0.3 pct Si. As discussed previously, the separate influences of Mn and Si will now be deduced from the published data listed in Table IX,[50,51,53–55] using linear regression. By using Eq. [30] as a reference, the data of Table IX were analyzed, leading to the following improvement, which takes the effects of Mn and Si concentration into account:

$$\log \mathrm{Nb} \times (\mathrm{C} + 12/14\ \mathrm{N}) = 2.26 + \frac{838\ \mathrm{Mn}^{0.246} - 1730\ \mathrm{Si}^{0.594} - 6440}{T} \qquad [31]$$

The measured solution temperatures are compared against those predicted by Eq. [31] in Figure 5. Here, it can be seen that the points follow the trend that takes the effects of Mn and Si additions into account. The previous equation will, therefore, be employed in all the calculations that follow.

2. *Modification to the DS Model*

In the present work, the expression for the constant A suggested by Bai[56] is also modified to allow for the effects of Mn and Si additions. Although the constant A has no direct physical meaning, it does depend on the chemical composition, or at least on the presence of elements that influence Nb mobility (*i.e.*, diffusivity) in austenite. As already discussed previously, Si and Mn affect the diffusivity

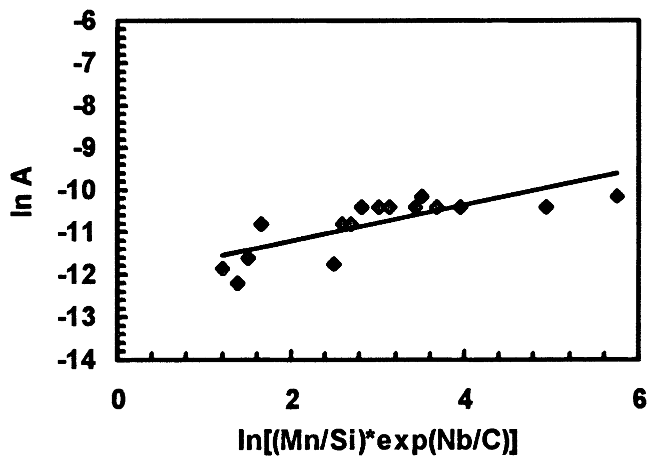

Fig. 6—Correlation between the coefficient A and the C, Mn, Si, and Nb contents.

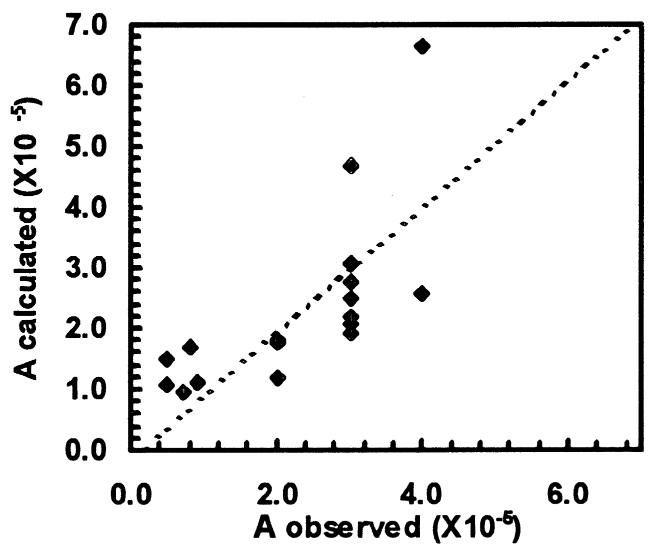

Fig. 7—Accuracy of Eq. [32].

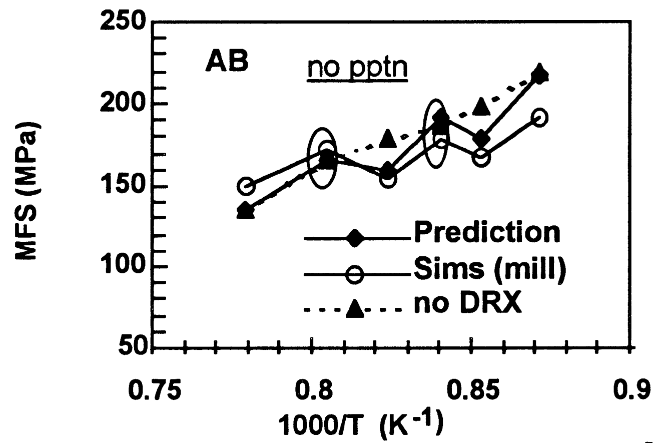

(*a*)

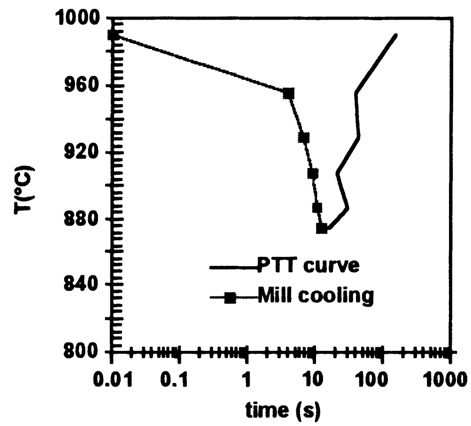

(*b*)

Fig. 8—(*a*) Comparison of MFS predictions and observations for the AB grade. The prediction indicates that precipitation does not take place during the schedule. As a result, DRX is considered to occur during the second and fourth passes, followed by MDRX. (*b*) Comparison of the precipitation-start curve with the mill cooling curve. According to the present analysis, precipitation does not occur.

of Nb and, therefore, the critical number of nuclei per unit volume. The latter quantity is included in the *A* constant, according to the derivation of the DS equation.

In the present investigation, the best overall fit to the mill logs was obtained by incorporating the dependence on exp (Nb/C) suggested by Bai together with a multiplying factor that depends on the Mn/Si ratio. The correlation found, with considerable spread, is illustrated in Figure 6. The expression that describes this behavior is as follows:

$$A = \frac{\left(\frac{\text{Mn}}{\text{Si}}\right)^{0.42} \exp\left(\frac{0.42\text{Nb}}{\text{C}}\right)}{169{,}400} \qquad [32]$$

The accuracy of the previous expression is illustrated in Figure 7, where the "observed" values are taken from the mill-log analyses described in more detail subsequently.

In addition to chemical composition, the previous processing history can also influence t_{ps}, according to Valdez and Sellars.[57] This factor can explain part of the large spreads observed during the analysis of mill logs. The precipitation kinetics depend not only on the parameters of finish rolling, but also on the reheat temperature and the characteristics of the roughing schedule. These two factors were not analyzed in the present study, and a more-detailed survey will be necessary to take these further factors into account.

According to the present method, a chart is generated which contains the mill cooling curve and the precipitation start time *vs* temperature curve. The intersection of the two curves defines the precipitation start point. This approach uses the additivity rule, proposed by Scheil,[58] to predict the time at which precipitation starts. The results lead to the conclusion that Mn retards the strain-induced precipitation of Nb(C, N), an effect that plays a role during the relatively short times involved in strip rolling. By contrast, Si has an *accelerating* effect on Nb(C, N) precipitation.[52] Two opposite cases are shown in Figures 8 and 9. The AB grade, which contains 0.031 pct Nb, 1.05 pct Mn, and 0.010 pct Si, displays *no* precipitation, whereas the MFS data for the AD6 grade, with 0.030 pct Nb, 0.65 pct Mn, and 0.010 pct Si, indicate that precipitation takes place between the third and fourth passes. The wide range of chemical compositions

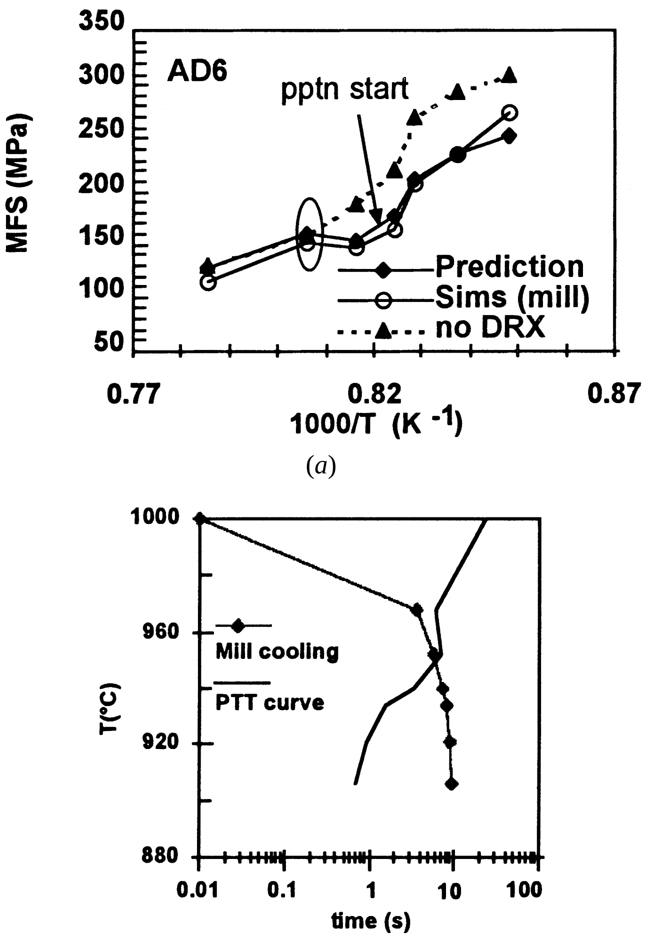

(b)

Fig. 9—(*a*) Comparison of MFS predictions and observations for the AD6 grade. The arrow indicates the precipitation start point. DRX is considered to occur during the second pass, followed by MDRX. (*b*) Comparison of the precipitation-start curve with the mill cooling curve. The point of intersection indicates the moment when precipitation starts.

shown in the table led to an isolation of the effects of Mn and Si in the present steels.

IV. ANALYSIS OF ROLLING SCHEDULES

The prediction of roll force during finish rolling is an important tool for the improvement of rolling schedules and of mill setups. An accurate model can also improve gage control and reduce the generation of scrap. The goal of this work was, therefore, to establish a method of predicting the MFS (and grain size) based on physical phenomena. Further details regarding individual aspects of this approach can be found in References 25, 27, 28, 32, 47, 52, 59, and 60.

It is useful to distinguish here between conventional-controlled rolling, where the aim is to produce work-hardened austenite, and DRX (+ MDRX)–controlled rolling, where the main purpose is to refine the austenite grain size. This work shows that both strategies are applicable to industrial strip rolling and that both intense grain refinement (initially) and strain accumulation (subsequently) can take place. Recent publications[21,22] by other workers indicate that DRX (+ MDRX) can be used to design schedules for the thermomechanical processing of steels when particular mechanical properties are desired.

In the results that follow, the MFS developed in each pass is derived from the mill logs. Here, corrections are used for the forward-slip ratio and the redundant strain, according to Reference 25. The MFSs are then predicted independently using the MFS model described in Section III–A, which takes into account the chemical composition as well as the occurrence of DRX + MDRX. In this way, the measured (mill log) MFS values can be compared to the predicted (model) MFS values. The microstructural model of Section III–B is then employed, together with the model that specifies the critical strain for the initiation of DRX (Section III–C). All the MFS calculations are based on the total strain (nominal + residual from the previous pass). For the Nb grades, the precipitation behavior during hot rolling is simulated using the model outlined in Section III–D. Examples are presented below of the behavior of each steel type, starting with the C-Mn grade, followed by the Cr-Mo grade, and ending with the microalloyed Nb grade.

For the plain C-Mn and Cr-Mo steels, the model predicts the MFS, grain size, amount of softening, and extent of DRX during the schedule, in a pass-by-pass analysis. For the Nb grades, the precipitation of niobium carbonitride is first predicted, which generally changes the behavior of the steel during rolling by preventing any further softening.

The Sims (*i.e.*, mill) and predicted MFS^+ values are plotted together with Misaka's MFS for all grades. However, the *accumulated strains* (calculated using the spreadsheet) are always employed to feed the Misaka equation. This allows the latter to fit the MFS curve more closely, especially when only small amounts of softening have taken place (common in the final passes, where the temperature is relatively low). The use of the original Misaka formulation with the *nominal* pass strain led to relatively poor fits.

The measured and predicted MFSs are plotted together and compared for each bar tested in this investigation.

A. *Plain C-Mn Steels*

The analysis of the rolling schedules of plain C-Mn grades is straightforward. In any particular pass, a strain is applied that results in softening during the interpass time and a characteristic grain size; the latter quantities act as inputs for the subsequent pass. The total strain is considered in the calculation of the MFS.

The plain C-Mn grades display a single type of behavior, one where DRX, followed by MDRX, occurs in the first passes. This is shown in Table X and Figure 10. The high temperatures and low strain rates involved decrease the peak strain, so that the critical strain for DRX is readily attained. Because no solute-drag elements (such as Nb) are present, the SRX and MDRX kinetics are rapid, as displayed. The fractional softening (X) during the interpass interval is always close to 1, for both the SRX and DRX + MDRX softening mechanisms. Nevertheless, the spreadsheet indicates that there is a small amount of strain accumulation in the final passes, due to the relatively low temperatures.

As shown in the corresponding MFS chart, the Misaka equation always overpredicts the MFS. This is due to the low Mn content of the grades considered here. Note that the model MFS^+ fits the Sims (mill) curve more closely, which demonstrates the effectiveness of the compositional term. There is no precipitation, and DRCR is occurring in the initial passes in all the bars analyzed here, causing most of

Table X. Grain Size, Fractional Softening, and MFS Predictions for the CS2 Grade

			C	0.45								
			Mn	0.76								
	Grade: CS2		Si	0.21								
Pass	d Entry (μm)	T (°C)	ε (s^{-1})	Ip Time (s)	ε	ε_a	ε_c	DRX?	$\varepsilon_{0.5}$	X_{dyn}	$t_{0.5}$ (s)	X
F 1	100.0	1043	4.5	8.60	0.95	0.95	0.30	yes	0.5	0.59	0.1	1.00
F 2	35.5	1000	12.0	4.45	0.83	0.83	0.31	yes	0.48	0.53	0.1	1.00
F 3	27.5	983	26.6	2.51	0.66	0.66	0.35	yes	0.50	0.35	0.0	1.00
F 4	22.8	957	49.5	1.56	0.54	0.54	0.41	yes	0.55	0.15	0.0	1.00
F 5	18.8	930	79.7	1.01	0.41	0.41	0.47	—	0.60	0	0.1	1.00
F 6	24.4	903	122.6	0.72	0.35	0.35	0.61	—	0.74	0	0.4	0.80
F 7	15.6	877	128.5	0.00	0.19	0.26	0.60	—	0.75	0	0.5	—

Pass	d if $X > 0.95$ MRX	SRX	Growth after MRX	SRX	1000/T (K^{-1})	MFS+ (MPa)	Sims (MPa)	Misaka (MPa)
F 1	30.2	33.8	35.5	51.1	0.76	115	99	139
F 2	20.7	21.6	27.5	40.8	0.79	139	129	170
F 3	15.4	20.4	22.8	34.3	0.80	157	168	187
F 4	11.5	19.0	18.8	28.5	0.81	179	180	208
F 5	8.8	18.2	13.3	24.4	0.83	196	209	225
F 6	6.8	19.8	6.0	15.6	0.85	216	206	247
F 7	6.2	18.2	15.6	15.6	0.87	221	226	253

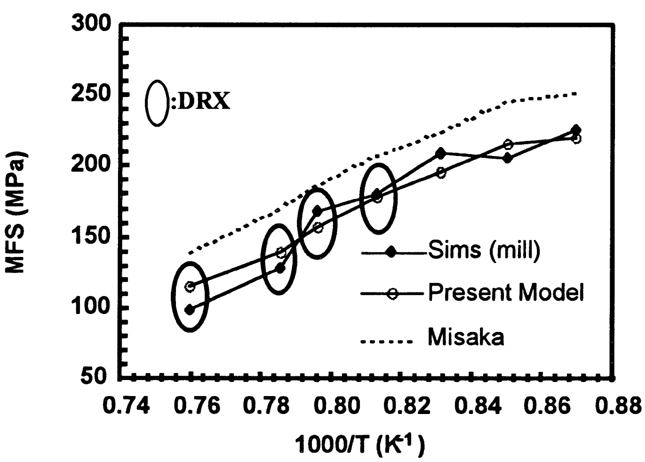

Fig. 10—MFS chart for grade CS2.

the grain refinement to occur in this part of the schedule (note the columns headed "d (μm)"). After the last pass, the simulated austenite grain size was about 15 μm for all grades.

B. *Cr-Mo Steels*

The Cr-Mo steels displayed MFS behaviors that were similar to those of the C-Mn steels. This is shown in Table XI and in Figure 11 for the BCM grade. The predicted MFSs are in excellent agreement with the MFS values calculated from the mill logs. For the present multiply alloyed grades, the ratio $\varepsilon_c/\varepsilon_p$ was set equal to 0.8, which was the ratio employed for the C-Mn steels.

The BCM grade is only lightly alloyed with Cr and Mo and, therefore, displays considerable softening during all the interpass intervals. These elements are not considered as severe recrystallization inhibitors, although they do have an effect on the kinetics.[32,51,61] The latter is taken into account *via* the $t_{0.5}$ equation. Additionally, DRX + MDRX takes place in the third pass, where the accumulated strain attains the critical strain for DRX. Compared to the plain C-Mn steels, the kinetics of recrystallization in the present multiply alloyed steels are about 10 times slower during static recrystallization (compare the $t_{0.5}$ columns for the C-Mn and Cr-Mo grades).

Figure 11 shows that the present model fits the Sims (mill) MFS data very well. This grade was rolled at relatively high temperatures. Nevertheless, even at these temperatures, the steel does not soften completely and some strain remains for the next pass, adding the residual to the newly applied strain. This seemed to occur during passes 1 and 2, and the MFS drop between passes 3 and 4 is successfully predicted and attributed to the occurrence of DRX + MDRX, due to strain accumulation. During the rest of the schedule, considerable strain is again accumulated. However, the critical strain increases proportionally, due to the higher strain rates and lower temperatures in the last passes, thus avoiding the initiation of DRX a second time.

It is evident from Table XI that dynamic recrystallization takes place in the present material due to the following.

(1) The rolling temperatures employed for these steels are higher than in the other materials, where finish rolling was initiated below 1000 °C. By contrast, in this schedule, the rolling temperature remained above 1000 °C within the first four or five stands.
(2) The strains employed in these particular schedules are higher than those used for the usual C-Mn and Nb steels, a condition that also promotes the occurrence of dynamic recrystallization.

It should be pointed out that, when no allowance is made for DRX and MRX in the model, *i.e.*, when the only softening mechanism that can operate is SRX, the predicted MFSs are clearly too high. This is because the times are too short at the low finishing temperatures involved for there to be significant softening by SRX. This important conclusion is

Table XI. Grain Size, Fractional Softening, and MFS Predictions for the BCM Grade

	C	0.28	V	Trace
	Mn	0.52	Nb	Trace
	Cr	0.38	N	0.0047
Grade: BCM	Ni	Trace	Mo	0.015

Pass	d Entry (μm)	T (°C)	$\dot{\varepsilon}$ (s^{-1})	Ip Time (s)	ε	ε_a	ε_c	DRX?	$\varepsilon_{0.5}$	X_{dyn}	$t_{0.5}$ (s)	X
F1	100.0	1098	5.24	18.53	0.83	0.83	1.00	—	4.46	0	8.80	0.77
F2	44.3	1052	10.43	4.39	0.61	0.80	0.86	—	6.96	0	3.61	0.57
F3	28.3	1028	22.77	2.55	0.65	0.99	0.85	yes	10.12	0.01	0.42	0.99
F4	20.2	1006	37.72	1.72	0.48	0.49	0.84	—	13.69	0	7.52	0.15
F5	19.2	983	57.72	1.17	0.39	0.81	0.95	—	19.74	0	2.59	0.27
F6	16.5	959	78.75	0.88	0.30	0.89	1.01	—	27.31	0	2.48	0.22
F7	14.6	934	81.83	—	0.18	0.87	1.05	—	35.67	0	2.69	

	d if $X > 0.95$		Growth after					
Pass	MRX	SRX	MRX	SRX	1000/T (K^{-1})	MFS$^+$ (MPa)	Sims (MPa)	Misaka (MPa)
F1	14.5	27.4	15.6	44.3	0.73	126	120	125
F2	11.8	16.2	13.8	28.3	0.75	150	145	142
F3	9.9	10.4	20.2	20.2	0.77	183	175	169
F4	8.5	13.3	15.4	19.2	0.78	176	181	179
F5	7.4	9.2	11.5	16.5	0.80	218	232	192
F6	6.5	7.8	10.9	14.6	0.81	245	247	202
F7	6.1	7.3	14.6	14.6	0.83	260	276	196

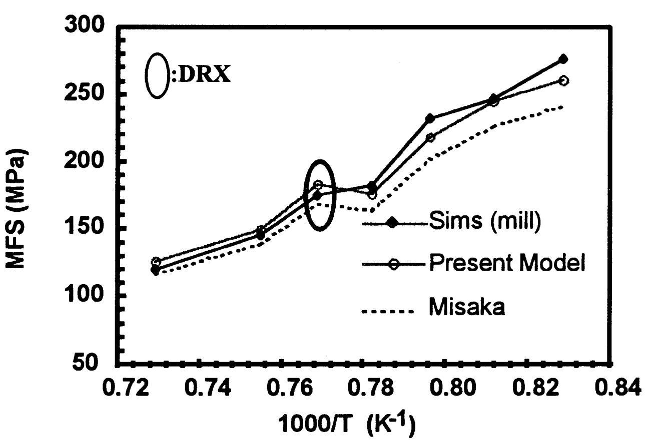

Fig. 11—MFS chart for grade BCM.

brought out more clearly in the examples considered subsequently.

C. *Nb Steels*

Analysis of the Nb steel mill data was by far the most complex. This is because it not only involves mechanisms such as SRX and DRX + MDRX, but the precipitation of Nb carbonitride as well. The occurrence of DRX + MDRX was mainly in the initial passes or after strain accumulation due to incomplete softening.

The Nb steels displayed a variety of rolling behaviors. For this reason, the grades are presented according to the operational softening mechanism (SRX or MDRX) and the occurrence, or lack, of precipitation. Four basic behaviors were observed in the group A steels: (1) SRX only and no precipitation, (2) SRX and DRX + MDRX and no precipitation, (3) SRX and DRX + MDRX and precipitation in the last passes, and (4) SRX and precipitation The results for each type observed are described in the following sections.

1. *SRX only and no precipitation*

Among all the bars analyzed, only two grades displayed SRX only and no precipitation: AD9 and AD10. These are the low-C and low-Nb (0.008 pct Nb) grades, and the results obtained for the AD9 grade are presented in Table XII and in Figure 12. They have the same base composition, with the exception of the Mn content. In both cases, the low Nb contents are responsible for this particular behavior. First, the critical strains are close to the ones applicable to C-Mn steels, and the total strains (nominal plus accumulated) are less than the critical strain for a given pass, thus avoiding the occurrence of DRX. According to the points discussed in Section III–C, the presence of Nb in solid solution at higher levels has a retarding effect on softening, increasing the peak strain and, therefore, increasing the critical strain. Second, no precipitation was predicted by the model. At this particular level of Nb, there is only a small driving force for precipitation, and t_{ps} was not attained, even in the final passes. The simulated MFS curve shown in Figure 12 is of the ascending type. It displays a fairly good fit to the Sims curve. Note that the original Misaka equation overpredicts the MFSs. For the low alloying levels used, this overprediction was expected.

Finally, it should be noted that there is little grain refinement, because softening occurs only by SRX, which refines the grain size less than DRX + MDRX. The final austenite grain size predicted in the two cases was about 30 μm.

2. *SRX and DRX + MDRX and no precipitation (DRX-controlled rolling)*

Considering a typical chemistry of a Nb grade, precipitation can be suppressed in several ways, *e.g.*, by increasing the rolling temperature, decreasing the Si level, increasing the Mn content, and also by schedule modifications. The

Table XII. Microstructural and MFS Predictions for the AD9 Grade

Grade: AD9

C	0.060
Mn	0.443
Nb	0.009
Si	0.010
Reheat T (°C) =	1215

Pass	d (μm)	T (°C)	ε (s^{-1})	Ip Time (s)	Time (s)	Z (s^{-1})	K_s	t_{ps} (s)	Sum t_{ip}/t_{ps}	PPTN?	ε	ε_a	ε_c	DRX?
F 1	80.0	1002	12.7	3.64	0.01	2.9×10^{16}	5.37	335.6	0.01	no	0.70	0.70	0.77	—
F 2	45.7	968	23.4	2.33	3.65	1.4×10^{17}	6.67	149.8	0.03	no	0.57	0.57	0.76	—
F 3	36.1	953	43.4	1.54	5.98	4.2×10^{17}	7.72	89.1	0.04	no	0.54	0.54	0.81	—
F 4	31.9	936	69.9	1.07	7.52	1.1×10^{18}	8.96	64.4	0.06	no	0.44	0.47	0.90	—
F 5	32.0	921	99.4	0.76	8.58	2.5×10^{18}	10.25	44.1	0.08	no	0.33	0.49	1.04	—
F 6	31.6	908	139.4	0.55	9.34	5.4×10^{18}	11.76	29.7	0.10	no	0.30	0.56	1.17	—
F 7	30.3	893	155.6	—	9.89	1.0×10^{19}	12.68	24.1	0.10	no	0.20	0.56	1.27	—

Pass	$\varepsilon_{0.5}$	X_{dyn}	$t_{0.5}$ (s)	X	d if $X > 0.95$		Growth after		1000/T (K^{-1})	MFS+ (MPa)	Sims (MPa)	Misaka (MPa)
					MRX	SRX	MRX	SRX				
F1	0.60	0	0.27	1.00	9.5	45.4	45.7	45.7	0.78	116	121	139
F2	0.61	0	0.32	0.99	8.0	36.0	36.1	36.1	0.81	128	126	154
F3	0.64	0	0.36	0.95	6.9	31.7	6.5	31.9	0.82	141	134	170
F4	0.68	0	0.68	0.66	6.1	32.0	7.2	32.0	0.83	151	157	182
F5	0.74	0	0.87	0.46	5.5	31.1	11.4	31.6	0.84	165	184	198
F6	0.80	0	0.82	0.37	5.0	28.1	13.8	30.3	0.85	182	191	219
F7	0.85	0	0.99	—	4.7	27.7	30.3	30.3	0.86	191	199	229

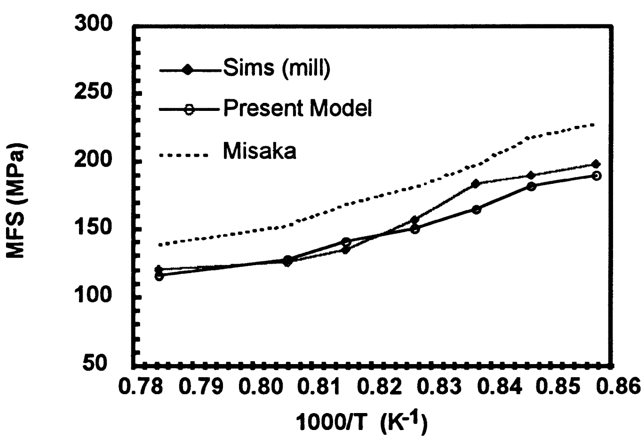

Fig. 12—MFS chart for grade AD9.

latter, by allowing sufficient softening between passes, prevents the strain accumulation required for the initiation of strain-induced precipitation. For the grades analyzed here, these conditions were occasionally observed in the MFS analysis, sometimes in association with each other. It is important to check the column "Sum t_{ip}/t_{ps}," which is a "measure" of the tendency for precipitation. When this ratio is greater than 1, by the additivity rule, precipitation is considered to occur.

Basically, there are two ways for DRX to take place during finishing. The first way is in the initial passes, where the high temperatures and low strain rates keep the critical strain low enough to be exceeded by the applied strain. The latter is usually large in the initial passes, because the steel is hotter. This situation is similar to the one applicable to the C-Mn grades. The other way for DRX to take place is to avoid softening by keeping the Nb in solid solution. After some strain accumulation due to incomplete softening between passes, if the Nb remains in solid solution, the total strain can exceed the critical strain, thereby initiating DRX. If precipitation occurs, however, the present model considers that there is no further softening. The grades that display SRX and DRX + MDRX behavior but no precipitation are AA1, AA2, AA3, AS1, AS2, AB, AD3, and AM1. Table XIII and Figure 13 (AS2 grade) display a typical example of this behavior. Note that the final grain sizes are quite small, especially if DRX occurs in the last passes, where the temperatures are low. In this case, the simulated austenite grain size is about 7 μm. This is caused by the intense grain refinement attributable to DRX.

The behavior of the AS2 grade is a good example of strain accumulation followed by dynamic softening. The small amounts of softening in the first two passes, attributable to the Nb in solution, caused the accumulated strain to rise to 1.38, which exceeded the critical strain of 1.33. The same mechanism was observed in pass 4, which led to DRX occurring during pass 5. The two DRX cycles resulted in MFS drops in the subsequent passes 4 and 6. The small addition of 0.016 pct Ti combines with most of the N at high temperatures, leaving the Nb largely in solid solution during finish rolling. This effect, associated with the high Mn (1.33 pct) and low Si (0.06 pct) contents, completely eliminated Nb carbonitride precipitation. According to Figure 13, the Sims (mill) MFS is well predicted by the present model. In this particular case, allowance for SRX as the sole static softening mechanism results in a severe overprediction of the MFS after the first cycle of DRX. On the other hand, Misaka's equation predicts the mill behavior quite well. This is because the high Mn level had increased the actual MFS, compensating for the generally observed overprediction of the Misaka relation. This demonstrates one more time the effectiveness of the chemical compositional term of the new MFS equation.

Table XIII. Microstructural and MFS Predictions for the AS2 Grade

	C	0.09
	Mn	1.33
Grade: AS2	Nb	0.036
	Si	0.060
(0.016 pct Ti)	Reheat T (°C) =	1215

Pass	d (μm)	T (°C)	ε (s^{-1})	Ip time (s)	Time (s)	Z (s^{-1})	K_s	t_{ps} (s)	Sum t_{ip}/t_{ps}	PPTN?	ε	ε_a	ε_c	DRX?
F1	80.0	1001	15.3	3.00	0.01	3.7×10^{16}	5.03	118.2	0.03	no	0.72	0.72	0.96	—
F2	78.1	961	24.7	2.05	3.01	1.8×10^{17}	7.14	22.6	0.12	no	0.50	1.10	1.12	—
F3	64.6	923	36.8	1.49	5.06	9.0×10^{17}	9.39	8.5	0.29	no	0.40	1.38	1.33	yes
F4	9.7	903	55.9	1.11	6.56	2.5×10^{18}	10.60	18.2	0.35	no	0.38	0.41	0.61	—
F5	9.6	898	85.9	0.83	7.67	4.6×10^{18}	11.79	7.9	0.46	no	0.36	0.77	0.68	yes
F6	6.6	882	109	0.65	8.50	1.0×10^{19}	14.05	13.7	0.50	no	0.30	0.36	0.64	—
F7	6.6	864	116	—	9.15	2.0×10^{19}	15.44	6.8	0.50	no	0.22	0.58	0.72	—

Pass	$\varepsilon_{0.5}$	X_{dyn}	$t_{0.5}$ (s)	X	d if $X > 0.95$ MRX	d if $X > 0.95$ SRX	Growth after MRX	Growth after SRX	1000/T (K^{-1})	MFS+ (MPa)	Sims (MPa)	Misaka (MPa)
F1	0.6	0	12.39	0.15	12.8	79.2	72.6	78.1	0.79	151	118	146
F2	0.7	0	12.31	0.11	10.5	50.3	62.5	64.6	0.81	190	169	184
F3	0.8	0	0.28	0.98	8.9	38.1	9.7	38.1	0.84	226	221	220
F4	0.6	0	47.24	0.01	8.0	24.0	9.6	9.6	0.85	195	201	188
F5	0.6	0.1	0.23	0.92	7.3	15.8	6.6	14.2	0.85	236	242	229
F6	0.6	0	300.54	0.00	6.6	20.2	6.6	6.6	0.87	217	230	210
F7	0.7	0	156.25	—	6.3	14.7	6.6	6.6	0.88	252	268	244

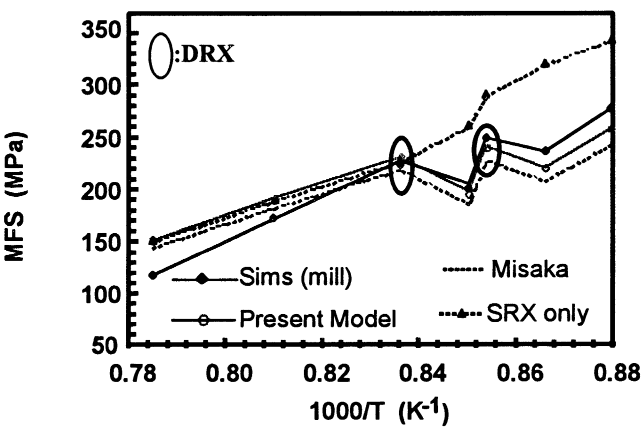

Fig. 13—MFS chart for grade AS2.

3. *SRX and DRX + MDRX and precipitation in the final passes*

The combination of DRX + MDRX followed by strain accumulation due to Nb carbonitride precipitation appears to be the most attractive schedule for hot strip rolling. This is because there is at least one DRX cycle somewhere in the early passes, which causes intense grain refinement. After that, precipitation occurs, which leads to full strain accumulation. The latter is desirable in order to produce a fine ferrite grain size after transformation. From a mill operational point of view, this type of behavior allows strain accumulation to be accomplished at relatively low rolling forces, because of the occurrence of DRX + MDRX early in the schedule.

The AD1, AD2, AD5, AD6, AD7, and AD8 grades displayed the aforementioned behavior in this analysis. The previous set includes two pairs of "coupled" steels: AD5 and AD6 and AD7 and AD8. Each pair involves a high-Si and low-Si version of the same base composition, which helps to establish the effect of Si addition. Grade AD8 is taken as an example here, as shown in Table XIV and in Figure 14.

Grade AD8 displays a DRX cycle in the second stand, due to the addition of the strain retained from the first pass due to incomplete softening. The austenite grain size is predicted to be about 17 μm. Grade AD8 is a low-Si steel, and precipitation was initiated between passes 3 and 4, according to the present analysis. The high-Si version experienced precipitation sooner for the same base composition and similar processing conditions (precipitation started between passes 2 and 3 for the high-Si version, grade AD7). At the end of the schedule, the retained strains were 1.52 in AD8 and 1.72 in the AD7 steel (in which precipitation began sooner). The Sims (mill) MFS curve is well predicted and, again, the Misaka MFS values are too high, partly because no allowance is made for DRX.

4. *SRX and precipitation (conventional-controlled rolling)*

Among all the Nb grades analyzed, there was a total absence of DRX in only three, according to the present model. The reductions in the initial passes were not large in these particular schedules, which is why the critical strain was not exceeded and why DRX was not initiated. The grades can be divided into two groups: the low-Nb AD4 and the two high-Nb grades, AD11 and AD12. The AD11 grade is represented by Table XV and by Figure 15.

Grade AD11 was rolled at relatively high temperatures, and considerable softening was observed during the interpass times before precipitation occurred. This led to some grain refinement, but not to the same extent as that produced by MDRX. The high Mn concentration (1.25 pct) delayed Nb carbonitride precipitation; nevertheless, because of the high Nb level, this occurred between the third and fourth passes.

Table XIV. Microstructural and MFS Predictions for the AD8 Grade.

	C	0.061
	Mn	0.699
	Nb	0.047
	Si	0.009
Grade: AD8	Reheat T (°C) =	1215

Pass	d (μm)	T (°C)	$\dot{\varepsilon}$ (s^{-1})	Ip Time (s)	Time (s)	Z (s^{-1})	K_s	t_{ps} (s)	Sum t_{ip}/t_{ps}	PPTN?	ε	ε_a	ε_c	DRX?
F 1	80.0	1001	14.5	3.55	0.01	3.4×10^{16}	5.32	20.1	0.18	no	0.85	0.85	0.89	—
F 2	66.9	967	25.8	2.26	3.56	1.6×10^{17}	6.65	5.5	0.59	no	0.56	1.13	1.06	yes
F 3	15.3	950	46.9	1.47	5.82	4.9×10^{17}	7.61	6.3	0.82	no	0.55	0.55	0.61	yes
F 4	16.8	937	84.2	0.95	7.30	1.3×10^{18}	8.31	2.9	1.14	yes	0.52	0.73	0.75	yes
F 5	16.8	931	141.1	0.62	8.24	2.6×10^{18}	9.21	1.3	1.58	yes	0.40	1.12	0.85	yes
F 6	16.8	915	172.8	0.44	8.87	5.3×10^{18}	10.74	0.8	2.08	yes	0.25	1.37	0.96	yes
F 7	16.8	899	179.6	—	9.31	9.4×10^{18}	11.62	0.6	2.08	yes	0.14	1.52	1.05	yes

Pass	$\varepsilon_{0.5}$	X_{dyn}	$t_{0.5}$ (s)	X	d if $X > 0.95$ MRX	SRX	Growth after MRX	SRX	1000/T (K^{-1})	MFS+ (MPa)	Sims (MPa)	Misaka (MPa)
F 1	0.60	0	6.24	0.33	9.3	39.9	38.4	66.9	0.78	130	112	148
F 2	0.68	0.136	0.19	1.00	7.8	29.3	15.3	15.3	0.81	160	154	180
F 3	0.52	0	1.05	0.62	6.8	17.7	5.8	16.8	0.82	152	150	173
F 4	0.58	0	1.21	0.00	6.1	15.6	16.8	16.8	0.83	179	169	204
F 5	0.61	0	1.02	0.00	5.5	11.6	16.8	16.8	0.83	213	208	242
F 6	0.67	0	1.29	0.00	5.0	10.2	16.8	16.8	0.84	235	238	268
F 7	0.72	0	1.46	—	4.8	9.5	16.8	16.8	0.85	250	284	284

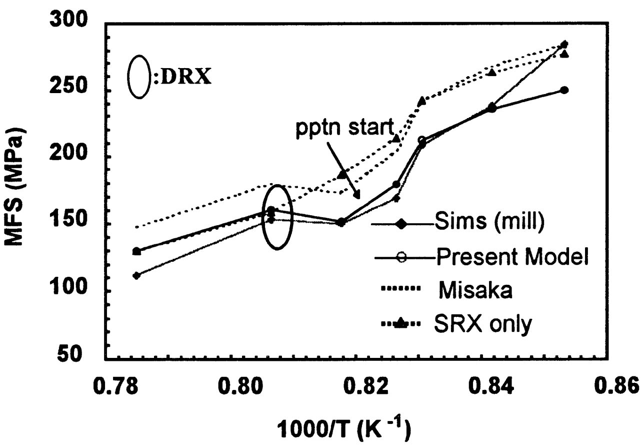

Fig. 14—MFS chart for grade AD8.

After precipitation starts, the strain was accumulated to 1.42. The absence of DRX agrees with the conclusions of Biglou *et al.*,[62] who studied the same grade, but under different conditions (torsion testing, low strain rates). The Sims (mill) MFS curves are well simulated for both grades. In this case, the Misaka equation also provides a good prediction, probably due to the high Mn level.

D. *The ferrite grain size after transformation*

The austenite grain size present after the last pass can be used as an input in a model for predicting the ferrite grain size. In their analysis of published data, Sellars and Beynon[63] derived a model that takes into account the retained strain, austenite grain size, and cooling rate. In the present demonstration, the cooling rate was taken as 20 °C/s for all grades. There are different parameters for C-Mn and Nb steels. For the Cr-Mo steels, the parameters for the C-Mn steels are used here. A typical calculation is described subsequently, where d_α^0 is the ferrite grain size when the austenite is unstrained (*i.e.*, recrystallized).

$$d_\alpha^0 = a + b\dot{T}^{-1/2} + c\,(1 - \exp\,(-1.5 \times 10^{-2}\, d_\gamma) \qquad [33]$$

where $\dot{T}$ is the cooling rate in °C/s, and d_γ is the austenite grain size. The parameters a, b, and c are given in Table XVI.

Because retained strain in the austenite reduces the ferrite grain size, it must be taken into account as well. This was done by using the following equation, where d_α is the ferrite grain size after transformation:

$$d_\alpha = d_\alpha^0\,(1 - 0.45\,\varepsilon_f^{1/2}) \qquad [34]$$

In this case, ε_f is the retained strain present in the material after leaving the finishing train. The ferrite grain size predicted for each grade analyzed here is given in Table XVII. According to the two ferrite grain-size equations referred to previously, the most important parameters that dictate the final size are the initial austenite grain size and the accumulated strain present before the strip is cooled on the runout table.

It can be seen that all the C-Mn grades display similar behaviors, residual strains (about 0.27), and austenite grain sizes (about 15 μm) and are, therefore, characterized by similar ferrite grain sizes (about 5.5 μm). The different schedule variations (*i.e.*, temperature, strain, strain rate, *etc.*) had little effect on the final result. Note that all the rolling simulations applied to these grades followed the DRX-controlled rolling paradigm.

The two Cr-Mo steels analyzed here were also "rolled" by DRX-controlled rolling methods, according to the model used in this study. However, there is more retained strain (0.87) in the BCM grade than in the BCMVN (0.58), due to the different cycles of DRX that apply to each schedule.

Table XV. Microstructural and MFS Predictions for the AD11 Grade

				C	0.06
				Mn	1.25
				Nb	0.075
Grade AD11				Si	0.325
(Ti: 0.024 pct)				Reheat T (°C) =	1215

Pass	d (μm)	T (°C)	ε (s^{-1})	Ip Time (s)	Time (s)	Z (s^{-1})	K_s	t_{ps} (s)	Sum t_p/t_{ps}	PPTN?	ε	ε_a	ε_c	DRX?
F 1	80.0	1023	13.3	3.50	0.00	1.7×10^{16}	5.10	20.46	0.17	no	0.60	0.60	0.83	—
F 2	40.4	992	22.2	2.35	3.50	6.9×10^{16}	6.91	7.86	0.47	no	0.50	0.63	0.74	—
F 3	20.4	958	33.1	1.70	5.85	2.7×10^{17}	8.78	4.25	0.87	no	0.41	0.48	0.67	—
F 4	20.0	943	45.6	1.28	7.55	5.9×10^{17}	10.06	2.69	1.35	yes	0.33	0.78	0.76	—
F 5	19.3	931	65.2	0.98	8.83	1.2×10^{18}	11.57	1.81	1.89	yes	0.30	1.08	0.86	—
F 6	18.8	916	74.8	0.76	9.81	2.2×10^{18}	13.63	1.39	2.44	yes	0.22	1.29	0.95	—
F 7	18.6	900	74.7	—	10.57	3.8×10^{18}	14.86	1.08	2.44	yes	0.13	1.42	1.04	—

Pass	$\varepsilon_{0.5}$	X_{dyn}	$t_{0.5}$ (s)	X	d if $X < 0.95$ MRX	d if $X < 0.95$ SRX	Growth after MRX	Growth after SRX	1000/T (K^{-1})	MFS+ (MPa)	Sims (MPa)	Misaka (MPa)
F 1	0.55	0	0.66	0.78	10.2	29.3	11.2	40.4	0.77	140	138	130
F 2	0.54	0	0.30	0.89	8.5	17.9	7.8	20.4	0.79	160	154	149
F 3	0.53	0	8.76	0.05	7.3	13.6	18.4	20.0	0.81	170	174	158
F 4	0.57	0	5.32	0.00	6.7	9.7	20.0	20.0	0.82	203	201	188
F 5	0.62	0	5.80	0.00	6.0	7.8	20.0	20.0	0.83	233	223	216
F 6	0.66	0	11.29	0.00	5.6	6.9	20.0	20.0	0.84	254	244	236
F 7	0.72	0	15.99	—	5.4	6.5	20.0	20.0	0.85	268	272	250

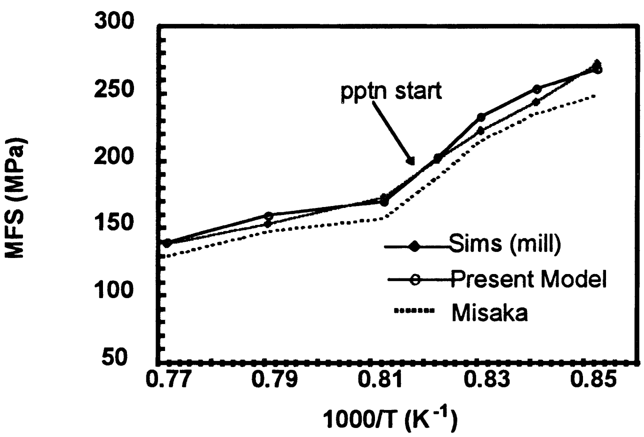

Fig. 15—MFS chart for grade AD11.

Table XVI. Parameters for Equation [33]

Steel	a	b	c
C-Mn	1.4	5.0	22
Nb	2.5	3.0	20

This difference affects the final ferrite grain size slightly, with an end result of about 4 μm for the BCM and 4.9 μm for the BCMVN grade.

There was more variation in the final ferrite grain sizes in the Nb grades, which fell in the range from 2.8 to 7.2 μm. Analyzing the data of Table XVII, it appears that the occurrence of DRX always produces fine ferrite grains (average size of 3.8 μm). The same can be said for the schedules in which DRX occurred in the initial passes, followed by precipitation (average size of 3.2 μm). Here, there was accumulated strain as well, which helped to maintain the ferrite grain sizes in the range from 2.8 to 3.8 μm.

Table XVII. Input Data, Type of Behavior, and Calculated Ferrite Grain Size for each Grade

Group	Grade	Schedule type	$d\gamma$	ε	d_α^0	d_α
A	AA1	DRCR	7.7	0.80	5.4	3.2
	AA2	DRCR	6.3	0.27	5.0	3.8
	AA3	DRCR	6.1	0.24	4.9	3.8
	AS1	DRCR	9.8	0.83	5.9	3.5
	AS2	DRCR	6.6	0.58	5.1	3.3
	AB	DRCR	7.4	0.59	5.3	3.5
	AD1	DRX + PPT	13.3	0.99	6.8	3.8
	AD2	DRX + PPT	10.4	1.26	6.1	3.0
	AD3	DRCR	17.4	0.70	7.8	4.8
	AD4	CCR	75.6	1.60	16.7	7.2
	AD5	DRX + PPT	16.5	1.93	7.6	2.8
	AD6	DRX + PPT	16.9	1.57	7.7	3.3
	AD7	DRX + PPT	15.9	1.72	7.4	3.0
	AD8	DRX + PPT	16.8	1.52	7.6	3.4
	AD9	SRX	30.3	0.56	10.5	7.0
	AD10	SRX	29.2	0.52	10.3	6.9
	AD11	CCR	18.6	1.42	8.0	3.7
	AD12	CCR	24.1	1.83	9.2	3.6
	AM1	DRCR	11.2	0.32	6.3	4.7
C	CA	DRCR	15.4	0.33	7.1	5.2
	CS1	DRCR	13.4	0.29	6.5	4.9
	CS2	DRCR	15.6	0.26	7.1	5.5
	CD	DRCR	16.9	0.22	7.4	5.9
	CM	DRCR	16.3	0.35	7.3	5.4
	CU	DRCR	15.4	0.26	7.1	5.4
B	BCM	DRCR	14.6	0.87	6.8	4.0
	BCMVN	DRCR	16.8	0.58	7.4	4.9

Only SRX was observed in the schedules applicable to grades AD9 and AD10; accordingly, the grain refinement was not so intense. The low strains and temperatures of the schedule and the low Nb level were responsible for this effect. The final austenite grain size was about 10 μm and the retained strain was about 0.5; this resulted in a ferrite grain size of about 7 μm, which is larger than average.

Conventional-controlled rolling leads to the presence of fine ferrite grains after transformation (average size of 4.8 μm). In grades AD11 and AD12, which had undergone relatively large strains in the initial passes, the austenite grain size was refined by SRX. Subsequently, precipitation led to strain accumulation, and these grades had large retained strains after the last pass (1.42 for AD11 and 1.83 for AD12); this state of affairs further contributed to refining the ferrite grain size. Another grade that underwent conventional-controlled rolling was AD4, which had received light reductions and in which no DRX occurred during the entire schedule. In this case, the grain refinement was poor.

The finest final grain size was produced in grade AD5, in which DRX occurred in the initial passes and precipitation in the final passes, leading to a large accumulation of strain. The retained strain further refined the ferrite grain size, to an extent comparable to the grades that had cycles of DRX during the schedule (DRX-controlled rolling).

V. CONCLUSIONS

An MFS model was developed to predict the strip-rolling behaviors of plain C-Mn, Cr-Mo, and Nb-bearing steels from the strains, strain rates, temperatures, and interpass times. It is based on an improved Misaka MFS equation and takes into account the quantities of the important alloying elements, the extent of recrystallization between passes, strain accumulation, and the possibility that DRX is initiated during a given pass. The following conclusions are drawn from this work.

1. The model indicates that DRX (followed by MDRX) occurs in the first few passes during the strip rolling of plain C-Mn grades. This is because the strains and temperatures are relatively high and the strain rates are quite low; thus, the DRX critical strain can be readily exceeded in these passes. It should be noted, however, that the type of DRX observed here is not associated with strain accumulation. This is in sharp contrast to the case of Nb-containing steels, where strain accumulation plays an important role.
2. The peak strain associated with the occurrence of DRX in Nb-containing steels can be characterized by including a term that reflects the Nb level. This expression is required for accurate prediction of the critical strain for the initiation of DRX. The equation indicates that strain accumulation leading to DRX (followed by MDRX) occurred in the later passes when some of the Nb steels studied were rolled. Thus, when MFS predictions are made only using SRX equations (a softening mechanism that does not operate during the later passes of rolling), the predicted MFS values are much higher than those measured in the mill.
3. The $\varepsilon_c/\varepsilon_p$ ratio decreases with increasing Nb content in the present steels. The elements Mn and Si have small (but not negligible) and opposite effects on the $\varepsilon_c/\varepsilon_p$ ratio. This ratio is important, because a clear understanding of the role of DRX in strip rolling requires use of the critical strain (rather than the peak strain) as a test of whether or not DRX is initiated.
4. For the Nb steels, whether DRX + MRX occurs in a given HSM depends on the Mn and Si levels (in addition to the C and Nb concentrations). It appears that the strain accumulation required to initiate DRX is more likely to take place when the Mn level is high (greater than 1.0 wt pct) and the Si level is low (less than 0.1 wt pct). These observations can be taken to imply that carbonitride precipitation is generally *absent* under the aforementioned conditions. Conversely, the presence of Si levels above about 0.1 wt pct is likely to provoke precipitation during rolling and, thus, prevent the initiation and propagation of DRX.
5. The previous observations indicate that Mn and Si have opposite effects on the rate of carbonitride precipitation. Increasing amounts of Si lead to faster kinetics, while increasing the Mn content retards the precipitation kinetics.
6. The precipitation start times applicable to strip mill rolling conditions can be predicted by modifying the DS equation so as to take the Mn and Si levels into account. This can then be incorporated into a model of the MFS behavior. The predictions obtained from the model described here are in good agreement with mill observations.
7. The MFS, microstructural and precipitation models derived or tuned with the aid of mill log data can be used to predict or interpret the metallurgical behavior of Nb steels during finish rolling.

ACKNOWLEDGMENTS

The authors are indebted to Mr. Brian Nelson, Dofasco Inc. (Hamilton, Canada), for supplying extensive hot strip mill rolling data. They express their special thanks to Professor Terrence M. Maccagno (University of Alberta, Edmonton, Canada), Mr. Koji Minami (Trico Steel Company, Decatur, AL), Mr. Atsushi Kirihata (Sumitomo Metal Industries, Wakayama, Japan), and Mr. Pascoal Bordignon (CBMM, Brazil) for numerous contributions to this research. They are also grateful to Mr. Brian McCrady (Algoma Inc., Sault Ste. Marie, Canada) and Dr. Chris Killmore of (BHP Steel, Port Kembla, Australia) for the provision of further mill logs. Financial support received from the Canadian Steel Industry Research Association (CSIRA) and the Natural Sciences and Engineering Research Council of Canada (NSERC) is acknowledged with gratitude. FS is grateful to the Conselho Nacional de Desenvolvimento Científico e Tecnologico, CNPq (Brazil), for the award of a doctoral scholarship.

LIST OF SYMBOLS AND PARAMETERS

ε	true strain
$\dot{\varepsilon}$	true strain rate (1/s)
ε_a	accumulated true strain
ε_c	critical strain for the initiation of dynamic recrystallization
ε_f	retained strain present in the material after leaving the finishing train
Z	Zener–Hollomon parameter $= \dot{\varepsilon} \cdot \exp\left(\frac{Q_{def}}{RT}\right)$ (1/s)

ε_p	peak strain
T	absolute temperature (K)
Q_{def}	activation energy for deformation (J/mol)
X	fractional softening
$t_{0.5}$	time for 50 pct softening (s)
R	gas constant = 8.31 (J/mol·K)
d_0	initial grain size (μm)
T_{nr}	interpass recrystallization stop temperature (K)
t_{ps}	precipitation start time
T_{RH}	absolute reheat temperature (K)
T_{pass}	absolute pass temperature (K)
T	cooling rate (°C/s)
H	strip thickness before passes
h	strip thickness after all passes
σ_M	mean flow stress
X_{dyn}	fractional softening attributable to dynamic recrystallization
σ_{ss}	steady-state stress
K	parameter that converts flow stress to mean flow stress
K_s	supersaturation ratio
t_{ip}	interpass time
Nb_{eff}	effective Nb concentration
d	grain size
d_α^o	ferrite grain size when the austenite is unstrained
d_γ	austenite grain size
d_α	ferrite grain size after transformation of deformed austenite

REFERENCES

1. F. Boratto, R. Barbosa, S. Yue, and J.J. Jonas: in *Thermec 88*, I Tamura, ed., ISIJ, Tokyo, 1988, pp. 383-89.
2. D.Q. Bai, S. Yue, and J.J. Jonas: *Proc. Int. Conf. on Modeling of Metal Rolling Processes*, The Institute of Materials, London, 1993, pp. 180-92.
3. D.Q. Bai, S. Yue, W.P. Sun, and J.J. Jonas: *Metall. Trans. A*, 1993, vol. 24A, pp. 2151-59.
4. T.M. Maccagno, J.J. Jonas, S. Yue, B.J. McCrady, R. Slobodian, and D. Deeks: *Iron Steel Inst. Jpn. Int.*, 1994, vol. 34, pp. 917-22.
5. *Microalloying '75*, Int. Symp. on HSLA Steels, Union Carbide Corp., New York, NY, USA, 1977.
6. M. Cohen and W. Owen: *Microalloying '75*, Int. Symp. on HSLA Steels, Union Carbide Corp., New York, NY, USA, 1977, pp. 2-8.
7. F.B. Pickering: *Microalloying '75*, Int. Symp. on HSLA Steels, Union Carbide Corp., New York, NY, USA, 1977, pp. 9-31.
8. T. Gladman, D. Dulieu, and I.D. McIvor: *Microalloying '75*, Int. Symp. on HSLA Steels, Union Carbide Corp., New York, NY, USA, 1977, pp. 32-58.
9. R.D. Stout: *Microalloying '75*, Int. Symp. on HSLA Steels, Union Carbide Corp., New York, NY, USA, 1977, pp. 488-97.
10. P.H.M. Hart, R.E. Dolby, N. Bailey, and D.J. Widgery: *Microalloying '75*, Int. Symp. on HSLA Steels, Union Carbide Corp., New York, NY, USA, 1977, pp. 540-51.
11. T.M. Maccagno, J.J. Jonas, and P.D. Hodgson: *Iron Steel Inst. Jpn. Int.*, 1996, vol. 36, pp. 720-28.
12. I.P. Kemp, P.D. Hodgson, and R.E. Gloss: *Proc. Int. Conf. on Modeling of Metal Rolling Processes*, The Institute of Materials, London, 1993, pp. 149-56.
13. T.M. Maccagno and J.J. Jonas: *Iron Steel Inst. Jpn. Int.*, 1994, vol. 34, pp. 607-14.
14. P.D. Hodgson: in *Thermec '97*, T. Chandra and T. Sakai, eds., TMS, Warrendale, PA, 1997, pp. 121-31.
15. P.D. Hodgson: Ph.D. Thesis, University of Queensland, Queensland, Australia, 1993, p. 3.
16. L.N. Pussegoda, P.D. Hodgson, and J.J. Jonas: *Mater. Sci. Technol.*, 1992, vol. 8, pp. 63-71.
17. L.N. Pussegoda, S. Yue, and J.J. Jonas: *Metall. Trans. A*, 1990, vol. 21A, pp. 153-64.
18. F.H. Samuel, S. Yue, J.J. Jonas, and B.A. Zbinden: *Iron Steel Inst. Jpn. Int.*, 1989, vol. 29, pp. 878-86.
19. E.C. Sarmento and J.F. Evans: *Proc. Int. Conf. on Processing, Microstructure and Properties of Microalloyed and Other High Strength Low Alloy Steels*, A.J. DeArdo, ed., ISS-AIME, Warrendale, PA, 1992, pp. 105-12.
20. J.J. Jonas: in *Recrystallization '90*, T. Chandra, ed., TMS-AIME, Warrendale, PA, 1990, pp. 27-36.
21. A. Schmitz, J. Neutjens, J.C. Herman, and V. Leroy: *40th MWSP Conf.*, ISS, Warrendale, PA, 1998, pp. 295-309.
22. J. Neutjens, P. Harlet, T. Bakolas, and P. Cantinieaux: *40th MWSP Conf.*, ISS, Warrendale, PA, 1998, pp. 311-21.
23. R.B. Sims: *Proc. Inst. Mech. Eng.*, 1954, vol. 168, pp. 191-200.
24. J.H. Hitchcock: *Roll Neck Bearings*, ASME, New York, NY, 1935, Appendix I, p. 33.
25. F. Siciliano, Jr., K. Minami, T.M. Maccagno, and J.J. Jonas: *Iron Steel Inst. Jpn. Int.*, 1996, vol. 36, pp. 1500-06.
26. Y. Misaka and T. Yoshimoto: *J. Jpn. Soc. Technol. Plast.*, 1967–68, vol. 8, pp. 414-22.
27. F. Siciliano, Jr.: Ph.D. Thesis, McGill University, Montreal, 1999, pp. 53-68.
28. K. Minami, F. Siciliano, Jr., T.M. Maccagno, and J.J. Jonas: *Iron Steel Inst. Jpn. Int.*, 1996, vol. 36, pp. 1507-15.
29. T. Senuma and H. Yada: *7th Risø Int. Symp.*, N. Hansen, D.J. Jensen, T. Leffers and B. Halph, Risø, Roskilde, Denmark, 1986, pp. 547-52.
30. H. Yada: *Proc. Int. Symp. on Accelerated Cooling of Rolled Steel*, G.E. Ruddle and A.F. Crawley, eds., Pergamon Press, Elmsford, NY, 1988, pp. 105-18.
31. T. Senuma, H. Yada, Y. Matsumura, and T. Futamura: *Tetsu-to-Hagané*, 1984, vol. 70, pp. 322-29 (in Japanese).
32. A. Kirihata, F. Siciliano, Jr., T.M. Maccagno, and J.J. Jonas: *Iron Steel Inst. Jpn. Int.*, 1998, vol. 38, pp. 187-95.
33. P.D. Hodgson and R.K Gibbs: *Iron Steel Inst. Jpn. Int.*, 1992, vol. 32, pp. 1329-38.
34. C. Roucoules, S. Yue, and J.J. Jonas: *Proc. Int. Conf. on Modeling of Metal Rolling Processes*, The Institute of Materials, London, 1993, pp. 165-79.
35. C. Roucoules: Ph.D. Thesis, McGill University, Montreal, 1992.
36. P.D. Hodgson, L.O. Hazeldon, D.L. Matthews, and R.E. Gloss: in *Microalloying '95*, M. Korchynsky, A.J. DeArdo, P. Repas and G. Tither, ISS–AIME, Warrendale, PA, 1995, pp. 341-53.
37. R.K. Gibbs, P.D. Hodgson, and B.A. Parker: in *Recrystallization '90*, T. Chandra, ed., TMS-AIME, Warrendale, PA, 1996, pp. 585-90.
38. J.J. Jonas and C.M. Sellars: in *Future Developments of Metals and Ceramics*, J.A. Charles, G.W. Greenwood and G.C. Smith, Institute of Materials, London, 1992, pp. 148-77.
39. D.C. Collinson, P.D. Hodgson, and C.H.J. Davies: *Thermec '97*, T. Chandra and T. Sakai, eds., TMS, Warrendale, PA, 1997, pp. 483-89.
40. C. Roucoules, S. Yue, and J.J. Jonas: *Metall. Mater. Trans. A*, 1995, vol. 26A, pp. 181-90.
41. P.D. Hodgson: *Mater. Sci. Technol.*, 1996, vol. 12, p. 788.
42. C.M. Sellars: *Mater. Sci. Technol.*, 1990, vol. 6, pp. 1072-81.
43. J.H. Beynon and C.M. Sellars: *Iron Steel Inst. Jpn. Int.*, 1992, vol. 32, pp. 359-67.
44. P.D. Hodgson, J.J. Jonas, and S. Yue: *Mater. Sci. Forum*, 1992, vols. 94–96, pp. 715-22.
45. M. Militzer, W.P. Sun, and J.J. Jonas: *Acta Metall. Mater.*, 1994, vol. 42, pp. 133-41.
46. C.M. Sellars: in *Hot Working and Forming Processes*, C.M. Sellars and G. Davies, eds., TMS, London, 1980, pp. 3-15.
47. F. Siciliano, Jr. and J.J. Jonas: in *Microalloying in Steels, Microalloying in Steels: New Trends, for the 21st Century*, CEIT, San Sebastian, Spain, J.M. Rodriguez-Ibabe, I. Gutierrez and B. Lopez, Trans-Tech Publications, Aedermannsdorf, 1998, p. 377; *Mater. Sci. Forum*, 1998, vols. 284–286, pp. 377-84.
48. S. Kurokawa, J.E. Ruzzante, A.M. Hey, and F. Dyment: *Met. Sci.*, 1983, vol. 17, pp. 433-38.
49. B. Dutta and C.M. Sellars: *Mater. Sci. Technol.*, 1987, vol. 3, pp. 197-206.
50. K.J. Irvine, F.B. Pickering, and T. Gladman: *J. Iron Steel Inst.*, 1967, vol. 205, pp. 161-82.
51. M.G. Akben, I. Weiss, and J.J. Jonas: *Acta Metall.*, 1981, vol. 29, pp. 111-21.
52. F. Siciliano, Jr., T.M. Maccagno, B.D. Nelson, and J.J. Jonas: *Thermec '97*, T. Chandra and T. Sakai, eds., TMS, Warrendale, PA, 1997, pp.

347-53.
53. L. Meyer: *Z. Metallkd.*, 1966, vol. 58, p. 334.
54. T.H. Johansen, N. Christensen and B. Augland: *Trans. AIME*, 1967, vol. 239, pp. 1651-54.
55. F. de Kazinsky, A. Axnas and P. Pachleitner: *Jernkont. Ann.*, 1963, vol. 147, p. 408.
56. D.Q. Bai: Ph.D. Thesis, McGill University, Montreal, 1995, pp. 28-32.
57. E. Valdez and C.M. Sellars: *Mater. Sci. Technol.*, 1991, vol. 7, pp. 622-30.
58. E. Scheil: *Arch. Eisenhüttenwes.*, 1935, vol. 12, p. 565 (cited in Ref. 56).
59. F. Siciliano, Jr. and J.J. Jonas: *ABM (Associação Brasileira de Metalurgia e Materiais)*, 1997, vol. 53, pp. 95-97 (in Portuguese).
60. F. Siciliano, Jr. and J.J. Jonas: *The 7th Int. Conf. on Steel Rolling*, Tokyo, Nov. 1998, pp. 534-39.
61. M.G. Akben and J.J. Jonas: *Proc. Int. Conf. on Technology and Applications of HSLA Steels*, ASM, Philadelphia, PA, 1983, pp. 149-61.
62. J.A. Biglou, B.D. Nelson, D.R. Hall, and J.G. Lenard: *37th MWSP Conf.*, ISS, Warrendale, PA, 1996, pp. 661-68.
63. C.M. Sellars and J.H. Beynon: *Proc. Conf. on HSLA Steels*, D.P. Dunne and T. Chandra, eds., South Coast Printers, Port Kembla, Australia, 1985, pp. 142-50.